PHYSICAL REVIEW D **73,** 053007 (2006)

Tenth-order QED contribution to the lepton $g-2$: Evaluation of dominant α^5 terms of muon $g-2$

Toichiro Kinoshita*
Laboratory for Elementary-Particle Physics, Cornell University, Ithaca, New York, 14853, USA

Makiko Nio†
Theoretical Physics Laboratory, RIKEN, Wako, Saitama, Japan 351-0198
(Received 18 January 2006; published 15 March 2006)

The QED contribution to the anomalous magnetic moments of electron and muon are known very precisely up to the order α^4. However, the knowledge of the α^5 term will also be required when the precision of measurement improves further. This paper reports the first systematic attempt to evaluate the α^5 term. Feynman diagrams contributing to this term can be classified into six gauge-invariant sets which can be subdivided further into 32 gauge-invariant subsets. Thus far we have numerically evaluated all integrals of 17 gauge-invariant subsets which contain light-by-light-scattering subdiagrams and/or vacuum-polarization subdiagrams. They cover most of leading terms of muon $g-2$ and lead to a preliminary result 663 (20) $(\alpha/\pi)^5$, which is 8.5 times more precise than the old estimate.

DOI: 10.1103/PhysRevD.73.053007 PACS numbers: 13.40.Em, 12.39.Fe, 12.40.Vv, 14.60.Ef

I. INTRODUCTION

The deviation of the electron g value from 2 predicted by Dirac's theory was first confirmed by an experiment on atomic spectrum [1]. Schwinger showed that this deviation can be explained as the effect of radiative correction by the relativistic renormalized QED which he had developed [2]. Together with the discovery of Lamb shift in the spectrum of hydrogen atom [3], it provided convincing experimental evidence that (until then discredited) QED is capable of predicting the effect of electromagnetic interaction precisely, provided that it is renormalized.

A. Measurement of electron $g-2$

By the 1970's the precision of measurement of electron $g-2$ was improved by four more orders of magnitude by means of spin precession of the electron moving in a constant uniform magnetic field [4]. The value of the electron $g-2$ was improved further by three additional orders of magnitude in a Penning trap experiment by Dehmelt's group at the University of Washington. Their published results are [5]

$$\begin{aligned} a_{e^-} &= 1\,159\,652\,188.4\,(4.3)\times 10^{-12}\ [3.8\ \text{ppb}], \\ a_{e^+} &= 1\,159\,652\,187.9\,(4.3)\times 10^{-12}\ [3.8\ \text{ppb}], \end{aligned} \tag{1}$$

where the numerals 4.3 in parentheses represent the combined statistical and systematic uncertainties in the last digits of the measured value. 1 ppb $= 10^{-9}$.

The precision of measurement has thus been improved by 7 orders of magnitude over 40 years. This enormous improvement in measurement was matched by the improvement of theory of radiative correction to the electron $g-2$ from the order α to the order α^4, leading to the most stringent test of the validity of QED.

The uncertainty of the experiment (1) was dominated by the cavity shift due to the interaction of the electron with the hyperboloid cavity, which has a very complicated resonance structure. Several efforts were made to reduced this uncertainty [6,7]. One of them is to replace the hyperboloid cavity by a cylindrical cavity, which allows analytic computation of the structure of the resonance [8]. Gabrielse's new measurement of the electron $g-2$ is based on this analysis. Recently a preliminary result of this measurement was reported, which is 7.5 times more precise than (1) [9].

B. Theory of electron $g-2$ to order α^4

The QED contribution to the electron g-2 can be written as

$$\begin{aligned} a_e(\text{QED}) = A_1 &+ A_2(m_e/m_\mu) + A_2(m_e/m_\tau) \\ &+ A_3(m_e/m_\mu, m_e/m_\tau) \end{aligned} \tag{2}$$

and A_i, $i=1,2,3$, can be expanded as

$$A_i = A_i^{(2)}\left(\frac{\alpha}{\pi}\right) + A_i^{(4)}\left(\frac{\alpha}{\pi}\right)^2 + A_i^{(6)}\left(\frac{\alpha}{\pi}\right)^3 + \ldots. \tag{3}$$

The first four coefficients of A_1 are

$$\begin{aligned} A_1^{(2)} &= 0.5, \qquad A_1^{(4)} = -0.328\,478\,965\ldots, \\ A_1^{(6)} &= 1.181\,241\,456\ldots, \qquad A_1^{(8)} = -1.7283\ (35). \end{aligned} \tag{4}$$

$A_1^{(2)}$ and $A_1^{(4)}$ are known analytically [2,10,11]. $A_1^{(6)}$ was obtained by both numerical [12] and analytic integrations [13]. $A_1^{(8)}$ is obtained thus far by numerical integration only [14]. Its uncertainty has been reduced by 10 compared with the old one [15]. Although it has been evaluated by one

*Electronic address: tk@hepth.cornell.edu
†Electronic address: nio@riken.jp

method only, it has been subjected to an extensive cross-checking among diagrams of 8th-order and also with 6th-, 4th-, and 2nd-order diagrams.

A_2 terms are small:

$$\begin{aligned} A_2^{(4)}(m_e/m_\mu)(\alpha/\pi)^2 &= 2.804 \times 10^{-12}, \\ A_2^{(4)}(m_e/m_\tau)(\alpha/\pi)^2 &= 0.010 \times 10^{-12}, \\ A_2^{(6)}(m_e/m_\mu)(\alpha/\pi)^3 &= -0.924 \times 10^{-13}, \\ A_2^{(6)}(m_e/m_\tau)(\alpha/\pi)^3 &= -0.825 \times 10^{-15} \end{aligned} \tag{5}$$

The contribution of A_3 term is even smaller ($\sim 2.4 \times 10^{-21}$). The non-QED contribution of the standard model are also known [16–18]

$$\begin{aligned} a_e(\text{hadron}) &= 1.671\,(19) \times 10^{-12}, \\ a_e(\text{weak}) &= 0.030\,(1) \times 10^{-12}. \end{aligned} \tag{6}$$

To compare the theory with the measured value of a_e one needs a value of α obtained by some non-QED measurement. The best available α at present is [19,20]

$$\alpha^{-1}(h/M_{C_s}) = 137.036\,000\,1\,(11)\ [7.4\ \text{ppb}]. \tag{7}$$

This leads to

$$\begin{aligned} a_e(h/M_{C_s}) &= 1\,159\,652\,175.86\,(0.10)(0.26)(8.48) \times 10^{-12}, \\ a_e(\text{exp}) - a_e(h/M_{C_s}) &= 12.4\,(9.5) \times 10^{-12}, \end{aligned} \tag{8}$$

where 0.10 is the remaining uncertainty of the α^4 term, 0.26 is based on an educated guess ($A_1^{(10)} = 0(3.8)$) made by Mohr and Taylor [20], and 8.48 is the uncertainty in the measurement (7). The error 8.48 is still large but is within a factor 2 of the error of the Seattle measurement (1).

C. Measurement of muon $g - 2$

The last and best of three measurements of the muon $g - 2$ at CERN had an uncertainty of 7 ppm [21]. After years of hard work the muon $g - 2$ measurement at the Brookhaven National Laboratory has come close to the design goal (0.35 ppm): [22]

$$a_{\mu^-}(\text{exp}) = 11\,659\,214\,(8)(3) \times 10^{-10}\ (0.7\ \text{ppm}). \tag{9}$$

The world average of $a_\mu(\text{exp})$ obtained by combining this and earlier measurements [21,23–25] is

$$a_\mu(\text{exp}) = 11\,659\,208\,(6) \times 10^{-10}\ (0.5\ \text{ppm}). \tag{10}$$

D. Hadronic and electroweak contributions to muon g-2

Currently, the prediction of the standard model reflects the difficulty in the treatment of the hadronic contribution [26–31]. The lowest-order hadronic vacuum-polarization effect on a_μ has thus far been determined from three sources,

(i) e^+e^- annihilation cross section,
(ii) hadronic τ decays,
(iii) $e^+e^- \to \gamma +$ hadrons [radiative return].

The process (i) has been analyzed by many groups over years. Some recent results are [32–34]

$$\begin{aligned} a_\mu(\text{had.LO}) &= 6934\,(53)_{\text{exp}}(36)_{\text{rad}} \times 10^{-11}, \\ a_\mu(\text{had.LO}) &= 6924\,(59)_{\text{exp}}(24)_{\text{rad}} \times 10^{-11}, \\ a_\mu(\text{had.LO}) &= 6944\,(48)_{\text{exp}}(10)_{\text{rad}} \times 10^{-11}. \end{aligned} \tag{11}$$

Recent estimate of hadronic light-by-light scattering contribution is [35]

$$a_\mu(\text{had.NL}) = 136\,(25) \times 10^{-11}. \tag{12}$$

The electroweak interaction effect is known to two-loop order: [36,37]

$$\begin{aligned} a_\mu(\text{weak}) &= 152\,(1) \times 10^{-11}, \\ a_\mu(\text{weak}) &= 154\,(1)(2) \times 10^{-11}, \end{aligned} \tag{13}$$

where (1) and (2) in the second line are estimates of remaining theoretical uncertainty and Higgs mass uncertainty, respectively.

E. QED contribution to muon g-2 to order α^4

The QED contribution to the muon g-2 can be written as

$$\begin{aligned} a_\mu(\text{QED}) = A_1 &+ A_2(m_\mu/m_e) + A_2(m_\tau/m_e) \\ &+ A_3(m_\mu/m_e, m_\tau/m_e). \end{aligned} \tag{14}$$

Renormalizability of QED guarantees that the functions A_1, A_2, and A_3 can be expanded in power series in α/π with finite calculable coefficients:

$$A_i = A_i^{(2)}\left(\frac{\alpha}{\pi}\right) + A_i^{(4)}\left(\frac{\alpha}{\pi}\right)^2 + A_i^{(6)}\left(\frac{\alpha}{\pi}\right)^3 + \ldots, \quad i = 1, 2, 3. \tag{15}$$

A_1 in (14) is identical with A_1 of (2) and has been evaluated to the eighth (i.e., α^4) order. As for A_2 and A_3, it is easy to see that $A_2^{(2)} = A_3^{(2)} = A_3^{(4)} = 0$ since they have no corresponding Feynman diagram. $A_2^{(4)}$, $A_2^{(6)}$, and $A_3^{(6)}$ terms have been evaluated accurately by power series expansion in m_e/m_μ or m_e/m_τ. Thus far $A_2^{(8)}$ and $A_3^{(8)}$ are known mostly by numerical integration.

The QED contribution $a_\mu(\text{QED})$, even though it is the predominant term of a_μ, has received little attention for many years because of its small error bars. The theoretical uncertainty came predominantly from the α^4 term whose contribution to a_μ is about 3.3 ppm. Recently we have completed a new evaluation of the α^4 term in which all contributing terms have been evaluated by two or more independent calculations, uncovering an error in some diagrams [38] and eliminating the α^4 term as a possible source of theoretical uncertainty [38,39]. This causes the

QED contribution to be shifted to

$$a_\mu(\mathrm{QED}) = 116\,584\,719.43\,(0.02)(1.15)(0.85) \times 10^{-11}, \tag{16}$$

where 0.02 is the remaining uncertainty of the α^4 term, an improvement of factor 40 over the previous result [15]. The uncertainty 1.15 comes from a crude estimate of the contribution of the α^5 term, which now stands out as the largest source of uncertainty in $a_\mu(\mathrm{QED})$. The error 0.85 comes from the uncertainty in the value of α given in (7).

The prediction of the standard model, including the hadronic vacuum-polarization, hadronic light-by-light contributions, and the electroweak effect, is

$$a_\mu(\mathrm{SM}) = 116\,591\,870.7\,(76.2) \times 10^{-11}, \tag{17}$$

where the uncertainty in theory is mostly due to the hadronic vacuum-polarization term.

F. Tenth-order term: Why is it needed?

A very important by-product of the study of a_e is that it gives the best value of the fine structure constant α available at present. If we use the new experiment by the Harvard group, the precision of α is almost an order of magnitude better than any other measurement of α.

Furthermore, the uncertainty of this measurement is only a factor 2 larger than that of theory, which is mostly from the α^5 term, since the α^4 term is known with small error. Thus, when the measurement of a_e is improved further, reduction of the uncertainty of α^5 term will become crucial in order to obtain a better $\alpha(a_e)$.

For the muon the old estimate of $A_2^{(10)}(m_\mu/m_e)$ was 930 (170), which contributes only 0.054 ppm to a_μ, well within the current experimental uncertainty. Thus improving $A_2^{(10)}(m_\mu/m_e)$ is not urgent. However, it will become an important source of error in the next generation of a_μ experiment. This is why it is desirable to obtain a better value of $A_2^{(10)}(m_\mu/m_e)$. The preliminary value of $A_2^{(10)}$ was reported in [40].

II. CLASSIFICATION OF TENTH-ORDER DIAGRAMS

Thus far only a small portion of tenth-order diagrams contributing to the muon $g-2$ have been evaluated analytically [41], or numerically [42]. Rough estimates based on the renormalization group and other considerations have been made in order to identify leading terms [42–45].

Of course an enormous amount of work is required to go beyond this and evaluate α^5 terms completely. Fortunately, for the muon $g-2$ the leading contribution comes from those Feynman diagrams which contain $\ln(m_\mu/m_e)$ terms whose sources can be readily identified as light-by-light-scattering subdiagrams and vacuum-polarization insertions. Thus a relatively modest amount of work will enable us to improve the value of $A_2^{(10)}(m_\mu/m_e)$ over the previous crude estimate. On the other hand, the electron $g-2$, in particular $A_1^{(10)}$ term, is much harder to evaluate. Besides its gigantic size none of 12 672 diagrams is dominant so that every term must be evaluated accurately.

For both a_e and a_μ the first step is to count and classify Feynman diagrams contributing to the α^5 term. The contribution to the mass-independent term $A_1^{(10)}$ may be classified into six gauge-invariant sets, which further subdivided into 32 gauge-invariant subsets, depending on the nature of subdiagrams (of the vacuum-polarization ($v-p$) type or light-by-light-scattering ($l-l$) type). Classification for $A_2^{(10)}(m_\mu/m_e)$ follows readily from that of $A_1^{(10)}$. With help of the Feynman Diagram autogenerator of GRACE system [46] we count the number of diagrams belonging to each set.

A. Notation

Vacuum-polarization functions Π needed for the evaluation of the α^5 contribution of the lepton $g-2$ may be classified as follows: In the following $\Pi_{x(y)}$ denotes a Π_x containing Π_y on its internal photon line.

Π_2, which consists of one closed lepton loop of second order.

Π_4, which consists of three proper lepton loops of fourth order.

$\Pi_{4(2)}$, which consists of three diagrams of type Π_4 in which one Π_2 is inserted in the internal photon line.

Π_6, which consists of 15 proper sixth-order lepton loops which do not contain $v-p$ loop.

$\Pi_{6(2)}$, which consists of 30 diagrams of type Π_6 in which one Π_2 is inserted in the internal photon line.

$\Pi_{4(4)}$, which consists of 9 diagrams of type Π_4 whose internal photon line contains a Π_4.

$\Pi_{4(2,2)}$, which consists of 3 diagrams of type Π_4 whose internal photon line contains two Π_2's.

Π_8, which consists of 105 proper eighth-order lepton loops.

Light-by-light scattering type functions Λ needed for the evaluation of the α^5 contribution of the lepton $g-2$ may be classified as follows:

Λ_4, which consists of six proper fourth-order lepton loop.

$\Lambda_4^{(2)}$, which consists of 60 diagrams in which lepton lines and vertices of Λ_4 are modified by second-order radiative corrections.

$\Lambda_4^{(4)}$, which consists of 105 diagrams in which lepton lines and vertices of Λ_4 are modified by fourth-order radiative corrections.

$\Lambda_{4(2)}^{(2)}$, which consists of 60 diagrams in which a $v-p$ diagram Π_2 is inserted in the photon line of $\Lambda_4^{(2)}$.

Λ_6, which consists of 120 proper lepton loops to which 6 photon lines are attached.

Finally we need magnetic moment contributions of various orders.

M_2, which consists of a lepton vertex diagram of second order.

M_4, which consists of six proper lepton vertices of fourth order.

M_6, which consists of 50 proper lepton vertices of sixth order.

M_{6LL}, which consists of 6 sixth-order vertex diagrams containing an *external* light-by-light loop Λ_4.

M_8, which consists of 518 proper lepton vertices of eighth-order which have no closed lepton loops.

M_{8LLb}, obtained by replacing Λ_4 by $\Lambda_4^{(2)}$ in M_{6LL}, and consists of 60 eighth-order vertex diagrams.

M_{8LLc}, obtained by attaching a virtual photon line to the open muon line in all possible ways, and consists of 48 eighth-order vertex diagrams.

M_{8LLd}, obtained by inserting a Λ_4 *internally* in the fourth-order M_4 in all possible ways.

B. Set I

Diagrams of Set I are built from the magnetic moment contribution M_2 of the second-order proper vertex. It consists of 208 Feynman diagrams, which can be classified further into ten gauge-invariant subsets as indicated in Fig. 1. Let us mention only contributions to $A_1^{(10)}$ and $A_2^{(10)}$ in this and subsequent sections although many subsets contribute also to $A_3^{(10)}$. This is because the contribution of $A_3^{(10)}$ is negligible compared with others.

Subset I(a).—Diagrams obtained by inserting four Π_2's in M_2. One Feynman diagram belonging to this subset contributes to $A_1^{(10)}$. The contribution to $A_2^{(10)}$ comes from 15 diagrams ($2^4 - 1 = 15$).

Subset I(b).—Diagrams obtained by inserting two Π_2's and one Π_4 in M_2. Nine Feynman diagrams of this subset contribute to $A_1^{(10)}$. The contribution to $A_2^{(10)}$ comes from 63 diagrams ($9(2^3 - 1) = 63$).

Subset I(c).—Diagrams containing two Π_4's in M_2. There are nine Feynman diagrams that contribute to $A_1^{(10)}$. The contribution to $A_2^{(10)}$ comes from 27 diagrams ($9(2^2 - 1) = 27$).

Subset I(d).—Diagrams obtained by insertion of one Π_2 and one $\Pi_{4(2)}$ in M_2. Six Feynman diagrams contribute to $A_1^{(10)}$. The contribution to $A_2^{(10)}$ comes from 42 diagrams ($6(2^3 - 1) = 42$).

Subset I(e).—Diagrams obtained by insertion of one Π_2 and one Π_6 in M_2. Thirty Feynman diagrams contribute to $A_1^{(10)}$. The contribution to $A_2^{(10)}$ comes from 90 diagrams ($30(2^2 - 1) = 90$).

Subset I(f).—Diagrams obtained by insertion of $\Pi_{4(2,2)}$ in M_2. The number of diagrams contributing to $A_1^{(10)}$ is 3. The contribution to $A_2^{(10)}$ comes from 21 diagrams ($3(2^3 - 1) = 21$).

Subset I(g).—Diagrams obtained by insertion of $\Pi_{4(4)}$ in M_2. The number of diagrams contributing to $A_1^{(10)}$ is 9. The contribution to $A_2^{(10)}$ comes from 27 diagrams ($9(2^2 - 1) = 27$).

Subset I(h).—Diagrams obtained by insertion of $\Pi_{6(2)}$ in M_2. The number of diagrams contributing to $A_1^{(10)}$ is 30. The contribution to $A_2^{(10)}$ comes from 90 diagrams ($30(2^2 - 1) = 90$).

Subset I(i).—Diagrams obtained by insertion of Π_8 in M_2. The number of diagrams contributing to $A_1^{(10)}$ is 105. The contribution to $A_2^{(10)}$ also comes from 105 diagrams.

Subset I(j).—Diagrams obtained by insertion of eighth-order photon propagators, which consist of two Λ_4's with three photons contracted, in M_2. The number of diagrams contributing to $A_1^{(10)}$ is 6. The contribution to $A_2^{(10)}$ comes from 18 diagrams ($6(2^2 - 1) = 18$).

The total number of diagrams of Set I contributing to $A_1^{(10)}$ is 208. The number of diagrams of Set I contributing to $A_2^{(10)}$ is 498.

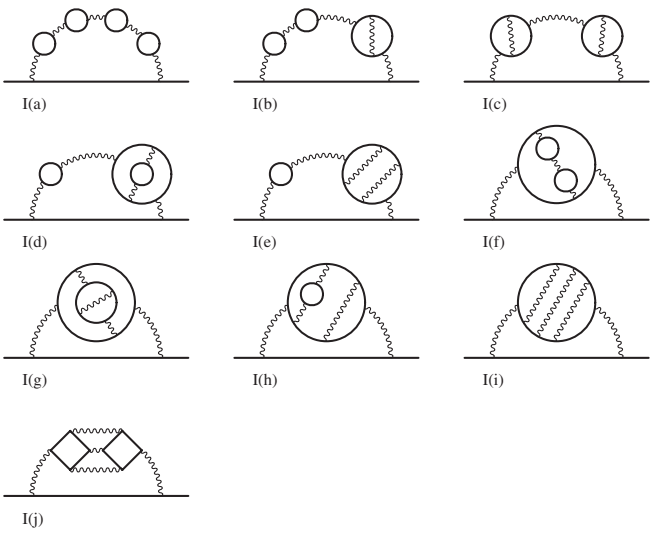

FIG. 1. Set I.

C. Set II

Diagrams of Set II are built upon six proper fourth-order vertices M_4 by insertion of various closed electron loops. It consists of 600 Feynman diagrams, which can be classified further into six gauge-invariant subsets as indicated in Fig. 2.

Subset II(a).—Diagrams obtained by inserting three Π_2's in M_4. The number of diagrams contributing to $A_1^{(10)}$ is 24. For the sake of programming convenience this set is subdivided into $\mathrm{II}(a_1)$, in which all three Π_2's are inserted in the same photon line, and $\mathrm{II}(a_2)$ in which Π_2 are on both photon lines. The total contribution to $A_2^{(10)}$ comes from 168 diagrams ($24(2^3 - 1) = 168$).

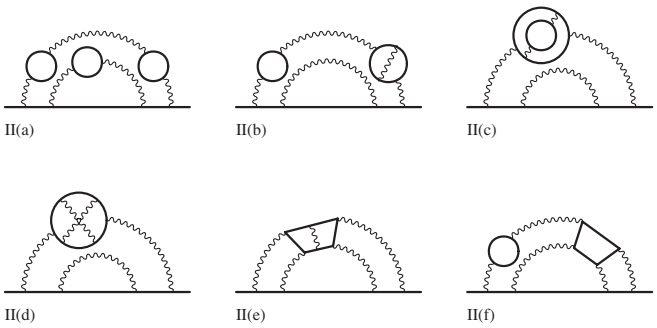

FIG. 2. Set II.

Subset II(b).—Diagrams obtained by inserting one Π_2 and one Π_4 in M_4. The number of diagrams contributing to $A_1^{(10)}$ is 108. The contribution to $A_2^{(10)}$ comes from 324 diagrams ($108(2^2-1)=324$).

Subset II(c).—Diagrams obtained by insertion of $\Pi_{4(2)}$ in M_4. The number of diagrams contributing to $A_1^{(10)}$ is 36. The contribution to $A_2^{(10)}$ comes from 108 diagrams ($36(2^2-1)=108$).

Subset II(d).—Diagrams obtained by insertion of Π_6 in M_4. The number of diagrams contributing to $A_1^{(10)}$ is 180. The contribution to $A_2^{(10)}$ comes also from 180 diagrams.

Subset II(e).—Diagrams obtained by insertion of internal light-by-light diagram $\Lambda_4^{(2)}$ in M_4. The number of diagrams contributing to $A_1^{(10)}$ is 180. The contribution to $A_2^{(10)}$ comes also from 180 diagrams.

Subset II(f).—Diagrams obtained by insertion of internal light-by-light diagram Λ_4 and additional Π_2 in M_4. The number of diagrams contributing to $A_1^{(10)}$ is 72. The contribution to $A_2^{(10)}$ comes from 216 diagrams ($72(2^2-1)=216$).

The total number of diagrams of Set II contributing to $A_1^{(10)}$ is 600. The number of diagrams of Set II contributing to $A_2^{(10)}$ is 1176.

D. Set III

Diagrams of Set III are built from 50 proper sixth-order vertices M_6 by insertion of various closed electron loops. This set consists of 1140 Feynman diagrams which can be classified further into three gauge-invariant subsets as indicated in Fig. 3 .

Subset III(a).—Diagrams obtained by inserting two Π_2's in M_6. The number of diagrams contributing to $A_1^{(10)}$ is 300. The contribution to $A_2^{(10)}$ comes from 900 diagrams ($300(2^2-1)=900$).

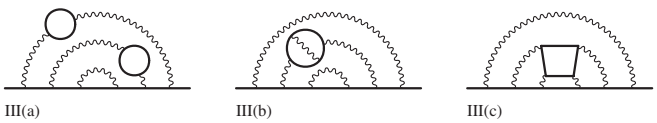

FIG. 3. Set III.

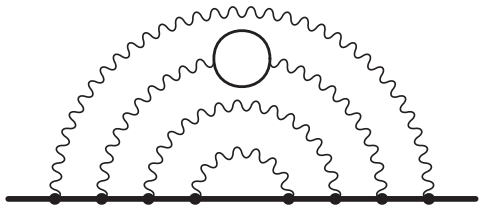

FIG. 4. Set IV.

Subset III(b).—Diagrams obtained by inserting Π_4 in M_6. The number of diagrams contributing to $A_1^{(10)}$ is 450. The contribution to $A_2^{(10)}$ comes also from 450 diagrams.

Subset III(c).—Diagrams obtained by insertion of an internal light-by-light diagram Λ_4 in M_6. The number of diagrams contributing to $A_1^{(10)}$ is 390. The contribution to $A_2^{(10)}$ comes also from 390 diagrams.

The total number of diagrams of Set III contributing to $A_1^{(10)}$ is 1140. The number of diagrams of Set II contributing to $A_2^{(10)}$ is 1740.

E. Set IV

Set IV is built from 518 proper eighth-order vertices M_8 by inserting a closed lepton loop of second order Π_2. It has only one subset. Total numbers of diagrams of Set IV contributing to $A_1^{(10)}$ and $A_2^{(10)}$ are both 2072. A representative diagram is shown in Fig. 4.

F. Set V

Set V consists of proper tenth-order vertices. It has only one subset consisting of 6354 diagrams and contributes only to $A_1^{(10)}$. A representative diagram is shown in Fig. 5.

G. Set VI

This set consists of vertex diagrams of various orders which contain at least one *l-l* subdiagram. Most diagrams of Set VI are built starting from the sixth-order diagram M_{6LL} which contains an external light-by-light-scattering subdiagram Λ_4. An exception is one subset that contains a subdiagram Λ_6. Note also that diagrams already contained in the Sets I, II, and III are excluded. The Set VI consists of 2298 Feynman diagrams which can be subdivided into 11 gauge-invariant subsets as indicated in Fig. 6.

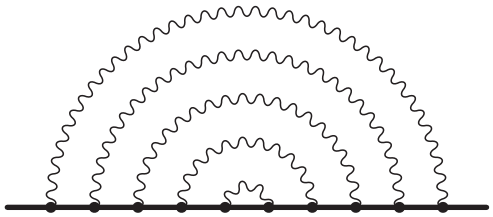

FIG. 5. Set V.

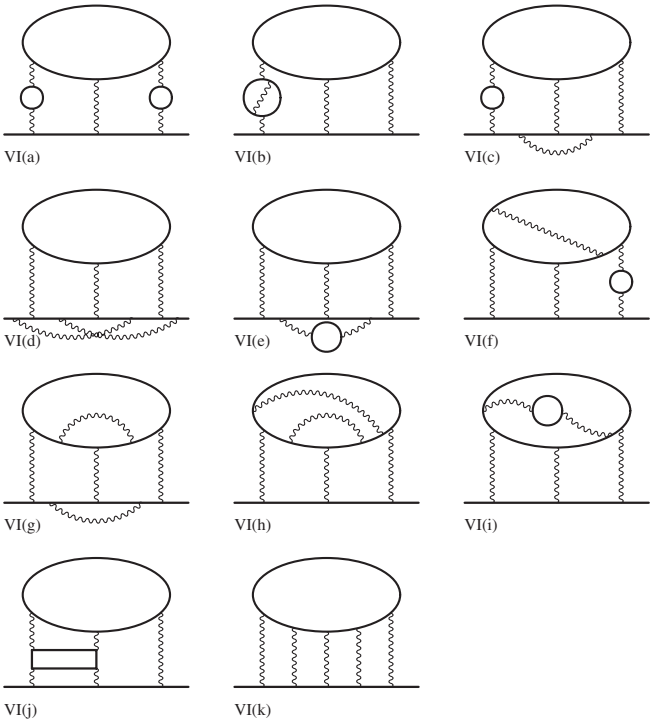

FIG. 6. Set VI.

Subset VI(a).—Diagrams obtained by inserting two Π_2's in the internal photon lines of M_{6LL}. The number of diagrams contributing to $A_1^{(10)}$ is 36. The contribution to $A_2^{(10)}$ comes from 252 diagrams ($36(2^3-1)=252$).

Subset VI(b).—Diagrams obtained by inserting a Π_4 in the internal photon lines of sixth-order diagram M_{6LL}. The number of diagrams contributing to $A_1^{(10)}$ is 54. The contribution to $A_2^{(10)}$ comes from 162 diagrams ($54(2^2-1)=162$).

Subset VI(c).—Diagrams obtained by inserting a Π_2 in the photon lines connecting the closed lepton loop Λ_4 and the open lepton line in the eighth-order diagrams M_{8LLc}. The number of diagrams contributing to $A_1^{(10)}$ is 144. The contribution to $A_2^{(10)}$ comes from 432 diagrams ($144(2^2-1)=432$).

Subset VI(d).—This subset consists of diagrams in which the open lepton line of M_{6LL} is modified by fourth-order radiative corrections. The number of diagrams contributing to $A_1^{(10)}$ is 492. The contribution to $A_2^{(10)}$ comes also from 492 diagrams.

Subset VI(e).—This subset consists of diagrams in which the open lepton line of M_{6LL} is modified by second-order radiative correction whose photon line has Π_2 insertion. The number of diagrams contributing to $A_1^{(10)}$ is 48. The contribution to $A_2^{(10)}$ comes from 144 diagrams ($48(2^2-1)=144$).

Subset VI(f).—This subset is derived from diagrams of M_{8LLb} in which photon lines connecting Λ_6 to the open lepton line receive a Π_2 insertion. The number of diagrams contributing to $A_1^{(10)}$ is 180. The contribution to $A_2^{(10)}$ comes from 540 diagrams ($180(2^2-1)=540$).

Subset VI(g).—This subset consists of diagrams in which both the closed loop Λ_4 and the open lepton line are modified by second-order radiative corrections. The number of diagrams contributing to $A_1^{(10)}$ is 480. The contribution to $A_2^{(10)}$ comes also from 480 diagrams.

Subset VI(h).—This subset consists of diagrams in which Λ_4 is modified by fourth-order radiative corrections. The number of diagrams contributing to $A_1^{(10)}$ is 630. The contribution to $A_2^{(10)}$ comes also from 630 diagrams.

Subset VI(i).—This subset consists of diagrams in which Λ_4 is modified by second-order radiative correction whose photon has a $v.p$ insertion Π_2. The number of diagrams contributing to $A_1^{(10)}$ is 60. The contribution to $A_2^{(10)}$ comes from 144 diagrams ($60(2^2-1)=180$).

Subset VI(j).—This subset is obtained from M_{6LL} (which contains a Λ_4) by hanging a second Λ_4 on two of three photon lines attached to the open lepton line. The number of diagrams contributing to $A_1^{(10)}$ is 54. The contribution to $A_2^{(10)}$ comes from 162 diagrams ($54(2^2-1)=162$).

Subset VI(k).—This subset consists of vertex diagrams containing Λ_6 five of whose photon lines end up on the open lepton line. The number of diagrams contributing to $A_1^{(10)}$ is 120. The contribution to $A_2^{(10)}$ comes also from 120 diagrams.

The total number of diagrams of Set VI contributing to $A_1^{(10)}$ is 2298. The number of diagrams of Set VI contributing to $A_2^{(10)}$ is 3594.

The total number of Feynman diagrams contributing to $A_1^{(10)}$ is the sum of contributions from all diagrams described above, which is 12 672. The total number for $A_2^{(10)}$ is 9080.

The number of Feynman diagrams contributing to $A_3^{(10)}$ can be readily derived from the above result.

III. LEADING DIAGRAMS CONTRIBUTING TO $a_\mu^{(10)}$

Fortunately, it is not difficult to identify diagrams which may give large contribution to $a_\mu^{(10)}$. They are diagrams containing $\ln(m_\mu/m_e)$ terms which tend to have large numerical values because m_μ is much larger than m_e.

One source of $\ln(m_\mu/m_e)$ is the vacuum-polarization contribution to the photon propagator which yields the logarithmic factor as a consequence of charge renormalization. The renormalized photon propagator has the form

$$D_R^{\mu,\nu}(q) = -i\frac{g^{\mu\nu}}{q^2}\,d_R(q^2/m_e^2,\alpha)+\cdots, \qquad (18)$$

where, to order α,

$$d_R(q^2/m_e^2, \alpha) = 1 + \frac{\alpha}{\pi}\left[\frac{1}{3}\ln(q^2/m_e^2) - \frac{5}{9} + \cdots\right]. \quad (19)$$

When D_R is inserted in $g-2$ diagrams, the momentum scale is set by the muon mass. Thus the α/π term will give a factor of the order of

$$K_\eta \equiv \frac{2}{3}\ln(\eta(m_\mu/m_e)) - \frac{5}{9}, \quad (20)$$

where η is an fuzzy factor of order 1. $K_\eta \simeq 3$ for $\eta = 1$.

As a matter of fact, more important sources of $\ln(m_\mu/m_e)$ are diagrams built up from the large sixth-order diagram M_{6LL} containing an *external* light-by-light scattering subdiagram of closed electron loop Λ_4. (By *external* we mean that one of four photon leg is the external magnetic field. If all photons are virtual photons, we call it *internal*.) The extraordinary size of M_{6LL} was initially discovered by numerical integration. The primary cause of large size is that it has a logarithmic mass-singularity for $m_e \to 0$. But this is not the whole story. It was pointed out by Yelikhoskii [44] that, in the large m_μ/m_e limit, the muon line may be regarded as a static source of Coulomb photons as well as hyperfine spin-spin interaction. Of three photons exchanged between the muon line and the electron loop, one photon is responsible for the spin-spin interaction while the other two are essentially static Coulomb potential. Integration over these Coulomb photon momenta gives a factor $i\pi$ each, contributing a factor $\pi^2(\sim 10)$ to the leading term

$$M_{6LL}^{(\text{leading})} = \frac{2\pi^2}{3}\ln(m_\mu/m_e). \quad (21)$$

For the physical value of m_μ/m_e, this is about 35. M_{6LL} as a whole is reduced by the negative mass-independent term to about 21, which is still very large. The value of M_{6LL} containing an electron loop Λ_4 is known exactly and its numerical value is [47]

$$M_{6LL} = 20.947\,924\,34\,(21), \quad (22)$$

where the uncertainty is due to that of the muon mass only.

The difference between M_{6LL} and $M_{6LL}^{(\text{leading})}$ may be interpreted as an indicator of the degree to which the picture of static Coulomb potential is valid. One way to incorporate this is to introduce a fudge factor ξ such that

$$M_{6LL} = \xi^2 M_{6LL}^{(\text{leading})}. \quad (23)$$

In this interpretation we have $\xi \simeq 0.77$.

These two sources of $\ln(m_\mu/m_e)$, light-light-scattering loop and vacuum-polarization loop, can work together and give even larger numerical factors. For instance, the leading term of the integral $A_2[\text{VI}(a)]$, which has insertion of two electron loops Π_2 and should have been written as VI(a)[e,e,e] following the notation of Table IV, will be of order [42]

$$A_2[\text{VI}(a)] \simeq 6K_\eta^2 M_{6LL}, \quad (24)$$

where the factor 6 is the number of ways two electron loops Π_2 can be inserted in M_{6LL}. This leads to $A_2[VI(a)] \simeq 1130$ for $\eta = 1$ ($K_\eta \simeq 3$). As is seen later, the actual value is about 543. Thus $K_\eta \sim 2$.

Similarly, the subset VI(b), which has insertion of one Π_4 in M_{6LL} (VI(b)[e,e] in the notation of Table IV), will give contribution of the order

$$A_2[\text{VI}(b)] \sim 3 \times \frac{3}{4} \times K_\eta M_{6LL} \simeq 142, \quad (25)$$

for $\eta = 1$ with the help of the identity [43]

$$\Pi_4(k^2) = \frac{\alpha}{\pi}\frac{3}{4}\Pi_2(k^2) + \left(\frac{\alpha}{\pi}\right)^2 k^2\left(\zeta(3) + \frac{5}{24}\right). \quad (26)$$

The numerical evaluation give $A_2[\text{VI}(b)] \simeq 169$. Thus $K_\eta \sim 3.5$ in this case.

If we apply blindly the argument based on (20), we would obtain, for $K_\eta \sim 3$,

$$\begin{aligned} A_2[\text{VI}(c)] &\simeq 3K_\eta M_{8LLc} \simeq 27, \\ A_2[\text{VI}(e)] &\simeq K_\eta M_{8LLc} \simeq 9, \\ A_2[\text{VI}(f)] &\simeq 3K_\eta M_{8LLb} \simeq -4.5, \\ A_2[VI(i)] &\simeq K_\eta M_{8LLb} \simeq -1.5. \end{aligned} \quad (27)$$

Unfortunately, these estimates are completely misleading because M_{8LLc} is the sum of large terms which tend to cancel each other. Similarly for M_{8LLb}.

Subsets VI(d), VI(g), and VI(j) have no Π_2 insertion and thus will have no particular enhancement although individual members of these subsets (being gauge-dependent) might have rather large values.

Among the diagrams of Sets I-V, the term with the highest power of logarithm is

$$A_2[\text{I}(a)] \sim \frac{8}{81}\ln^4(m_\mu/m_e), \quad (28)$$

although its value (~ 80) is not dominating because of its small numerical factor. Actually terms of lower logarithmic powers reduce this to an even smaller value (~ 20).

In the study of eighth-order terms, the value of K_η was found to be smaller than 3 in most cases and varies in the range $2 < K_\eta < 2.5$, except for VI(b). Thus the estimates given above for $\eta = 1$ (or $K_\eta \sim 3$) are likely to be overestimates by $20 \sim 50\%$.

The contribution of the subset VI(k) had been estimated in a different manner. It is shown [44] that the leading term in the large m_μ/m_e limit is of the form

$$A_2[\text{VI}(k)] = \pi^4(0.438\ldots\ln(m_\mu/m_e) + \ldots). \quad (29)$$

Based on this observation it was estimated that [43]

$$A_2[\text{VI}(k)] \simeq 185 \pm 85. \quad (30)$$

This term is large mainly because of the presence of the π^4 factor. Its origin can be readily understood by a generalization of the argument leading to Eq. (21) to the case in which $2n+1$ photons are exchanged between the light-by-light type loop Λ_{2n+2}, $n = 1, 2, \ldots$, and the muon line [44]. In the large m_μ/m_e limit this mechanism generates the structure

$$A_2^{(2n+1)} \simeq c_n \pi^{2n} \ln(m_\mu/m_e) + \cdots. \tag{31}$$

Numerical values of some c_n are known [48]

$$c_1 = \frac{2}{3}, \qquad c_2 = 0.438\ldots. \tag{32}$$

IV. ANALYTICALLY KNOWN CONTRIBUTION TO $a_\mu^{(10)}$

At present only a small number of integrals in the subsets I(a), I(b), I(c), II(a), and II(b) are known analytically. Their expansion in the ratio m_e/m_μ are given in [41]. From Table 2 of [41] we obtain

$$\begin{aligned} a_\mu[\mathrm{I}(a)] &= 22.566973\,(3), \\ a_\mu[\mathrm{I}(b)] &= 30.667091\,(3), \\ a_\mu[\mathrm{I}(c)] &= 5.141395\,(1), \\ a_\mu[\mathrm{II}(a)] &= -36.174859\,(2), \\ a_\mu[\mathrm{II}(b)] &= -23.462173\,(1), \end{aligned} \tag{33}$$

where the uncertainties come from the measurement uncertainty of m_e/m_μ only. These results show strong cancellation among diagrams of Sets I and II, which is analogous with the cancellation among Group I and Group II diagrams contributing to the eighth-order term of muon $g-2$.

V. NUMERICAL EVALUATION OF DIAGRAMS CONTRIBUTING TO $a_\mu^{(10)}$

As was discussed in Sec. II diagrams containing light-by-light-scattering subdiagrams, namely, the Set VI, is the source of dominant contribution to $a_\mu^{(10)}$. However, let us describe the results of numerical evaluation starting from the Set I.

A. Set I

Integrals for the diagrams of Set I, except for subsets I(i) and I(j), can be readily obtained from eighth-order diagrams belonging to Group I by insertion of $v-p$ loops. Diagrams numerically evaluated thus far are shown in Tables I, II, and III. Summing up the first four lines of Table I one obtains

$$\begin{aligned} A_2[I(a)] &= M_{2,p2:4}^{(e,e,e,e)} + M_{2,p2:4}^{(e,e,e,m)} + M_{2,p2:4}^{(e,e,m,m)} + M_{2,p2:4}^{(e,m,m,m)} \\ &= 22.567\,05\,(25). \end{aligned} \tag{34}$$

TABLE I. Numerical evaluation of diagrams of subsets (a), (b), (c), and (e) of Set I. The notation follows that of [42] with some modification and adaptation. n_F is the number of Feynman diagrams represented by the integral.

Integral	n_F	Value (error) including n_F	Sampling per iteration	No. of iterations
$M_{2,p2:4}^{(e,e,e,e)}$	1	20.142 93 (23)	1×10^8	180
$M_{2,p2:4}^{(e,e,e,m)}$	4	2.203 27 (9)	1×10^7	80
$M_{2,p2:4}^{(e,e,m,m)}$	6	0.20 697 (2)	1×10^7	20
$M_{2,p2:4}^{(e,m,m,m)}$	4	0.013 88 (1)	1×10^7	20
$M_{2,p2:4}^{(m,m,m,m)}$	1	$4.7094\,(6)\times10^{-4}$	1×10^7	20
$M_{2,p4,p2:2}^{(e,e,e)}$	9	27.690 38 (30)	4×10^8	190
$M_{2,p4,p2:2}^{(e,m,e)}$	18	1.166 28 (9)	1×10^7	100
$M_{2,p4,p2:2}^{(e,m,m)}$	9	0.031 82 (3)	1×10^6	20
$M_{2,p4,p2:2}^{(m,e,e)}$	9	1.614 36 (6)	1×10^7	120
$M_{2,p4,p2:2}^{(m,m,e)}$	18	0.164 70 (5)	1×10^6	20
$M_{2,p4,p2:2}^{(m,m,m)}$	9	$7.0108\,(7)\times10^{-3}$	1×10^7	20
$M_{2,p4:2}^{(e,e)}$	9	4.742 12 (14)	1×10^8	220
$M_{2,p4:2}^{(e,m)}$	18	0.399 26 (3)	1×10^7	120
$M_{2,p4:2}^{(m,m)}$	9	$2.3468\,(2)\times10^{-2}$	1×10^7	20
$M_{2,p6p2}^{(e,e)}$	30	−1.208 41 (70)	1×10^8	100
$M_{2,p6p2}^{(e,m)}$	30	−0.021 10 (4)	1×10^7	120
$M_{2,p6p2}^{(m,e)}$	30	0.010 31 (1)	1×10^6	20
$M_{2,p6p2}^{(m,m)}$	30	$1.0296\,(4)\times10^{-2}$	1×10^7	20

TABLE II. Numerical evaluation of diagrams of subsets (d) of Set I. The notation follows that of [42] with some modification and adaptation. n_F is the number of Feynman diagrams represented by the integral. Subscripts $p4A$, $p4B$ refer to part of fourth-order $v - p$ Π_4 containing vertex correction and self-energy insertion, respectively. The last four lines are values obtained using the exact sixth-order spectral function $\Pi_{4(2)}$.

Integral	n_F	Value (error) including n_F	Sampling per iteration	No. of iterations
$M_{2,p4A(p2)p2}^{(e(e),e)}$	2	2.630 64 (72)	1×10^7	80
$M_{2,p4A(p2)p2}^{(m(e),e)}$	2	0.769 97 (7)	1×10^7	40
$M_{2,p4A(p2)p2}^{(e(m),e)}$	2	0.127 03 (2)	1×10^7	40
$M_{2,p4A(p2)p2}^{(m(m),e)}$	2	$7.3352\,(7) \times 10^{-2}$	1×10^7	40
$M_{2,p4A(p2)p2}^{(e(e),m)}$	2	$1.3211\,(18) \times 10^{-2}$	1×10^7	79
$M_{2,p4A(p2)p2}^{(m(e),m)}$	2	$3.5428\,(4) \times 10^{-2}$	1×10^7	40
$M_{2,p4A(p2)p2}^{(e(m),m)}$	2	$5.0276\,(6) \times 10^{-3}$	1×10^7	40
$M_{2,p4A(p2)p2}^{(m(m),m)}$	2	$3.8330\,(4) \times 10^{-3}$	1×10^7	40
$M_{2,p4B(p2)p2}^{(e(e),e)}$	4	5.51053 (70)	1×10^7	80
$M_{2,p4B(p2)p2}^{(m(e),e)}$	4	0.634 90 (9)	1×10^7	40
$M_{2,p4B(p2)p2}^{(e(m),e)}$	4	$3.9114\,(47) \times 10^{-3}$	1×10^7	29
$M_{2,p4B(p2)p2}^{(m(m),e)}$	4	$1.1129\,(4) \times 10^{-2}$	1×10^7	29
$M_{2,p4B(p2)p2}^{(e(e),m)}$	4	0.157 98 (2)	1×10^7	80
$M_{2,p4B(p2)p2}^{(m(e),m)}$	4	$3.2133\,(5) \times 10^{-2}$	1×10^7	40
$M_{2,p4B(p2)p2}^{(e(m),m)}$	4	$2.6449\,(19) \times 10^{-4}$	1×10^7	40
$M_{2,p4B(p2)p2}^{(m(m),m)}$	4	$6.1873\,(17) \times 10^{-4}$	1×10^7	40
$M_{2,p4(p2)p2}^{(e(e),e)}$	6	7.452 70 (88)	1×10^8	140
$M_{2,p4(p2)p2}^{(e(e),m)}$	6	0.158 53 (10)	1×10^7	120
$M_{2,p4(p2)p2}^{(m(m),e)}$	6	0.071 73 (3)	1×10^6	20
$M_{2,p4(p2)p2}^{(m(m),m)}$	6	$3.8028\,(5) \times 10^{-3}$	1×10^7	20

TABLE III. Numerical evaluation of diagrams of subsets (f) of Set I. The notation follows that of [42] with some modification and adaptation. n_F is the number of Feynman diagrams represented by the integral. Subscripts $p4A$, $p4B$ refer to part of fourth-order $v - p$ Π_4 containing vertex correction and self-energy insertion, respectively.

Integral	n_F	Value (error) including n_F	Sampling per iteration	No. of iterations
$\Delta M_{2,p4A(p2:2)}^{(e(e,e))}$	1	1.997 47 (10)	4×10^7	240
$\Delta M_{2,p4A(p2:2)}^{(e(e,m))}$	2	0.158 63 (3)	1×10^7	20
$\Delta M_{2,p4A(p2:2)}^{(e(m,m))}$	1	$1.0612\,(2) \times 10^{-2}$	1×10^7	20
$\Delta M_{2,p4A(p2:2)}^{(m(e,e))}$	1	0.44 361 (6)	1×10^7	20
$\Delta M_{2,p4A(p2:2)}^{(m(e,m))}$	2	$9.4542\,(13) \times 10^{-2}$	1×10^7	20
$\Delta M_{2,p4A(p2:2)}^{(m(m,m))}$	1	$8.1763\,(13) \times 10^{-3}$	1×10^7	20
$\Delta M_{2,p4B(p2:2)}^{(e(e,e))}$	2	0.949 59 (11)	1×10^7	340
$\Delta M_{2,p4B(p2:2)}^{(e(e,m))}$	4	$2.5573\,(56) \times 10^{-3}$	1×10^7	20
$\Delta M_{2,p4B(p2:2)}^{(e(m,m))}$	2	$1.6448\,(275) \times 10^{-5}$	1×10^7	20
$\Delta M_{2,p4B(p2:2)}^{(m(e,e))}$	2	0.260 23 (6)	1×10^7	20
$\Delta M_{2,p4B(p2:2)}^{(m(e,m))}$	4	$1.1060\,(5) \times 10^{-2}$	1×10^7	20
$\Delta M_{2,p4B(p2:2)}^{(m(m,m))}$	2	$2.6957\,(32) \times 10^{-4}$	1×10^7	20

Similarly, we find from the rest of Table I

$$\begin{aligned} A_2[I(b)] &= M^{(e,e,e)}_{2,p4,p2:2} + M^{(e,m,e)}_{2,p4,p2:2} + M^{(e,m,m)}_{2,p4,p2:2} \\ &\quad + M^{(m,e,e)}_{2,p4,p2:2} + M^{(m,m,e)}_{2,p4,p2:2} \\ &= 30.667\,54(33), \\ A_2[I(c)] &= M^{(e,e)}_{2,p4:2} + M^{(e,m)}_{2,p4:2} \\ &= 5.141\,38\,(15), \end{aligned} \tag{35}$$

The values of $A_2[\mathrm{I}(a)]$, $A_2[\mathrm{I}(b)]$, and $A_2[\mathrm{I}(c)]$ are in good agreement with semianalytic values [41] quoted in (33).

$A_2[\mathrm{I}(d)]$ is evaluated from the entries in Table II together with Table III and Table VI of [39], which list residual renormalization terms. We obtain

$$\begin{aligned} M^{(e(e),e)}_{2,p4(p2)p2} &= 2M^{(e(e),e)}_{2,p4A(p2)p2} + 4M^{(e(e),e)}_{2,p4B(p2)p2} \\ &\quad - 4\Delta B^{(e,e)}_{2,p2} M^{(m,e,e)}_{2,p2:2} \\ &= 7.451\,73\,(101), \\ M^{(m(e),e)}_{2,p4(p2)p2} &= 2M^{(m(e),e)}_{2,p4A(p2)p2} + 4M^{(m(e),e)}_{2,p4B(p2)p2} \\ &\quad - 4\Delta B^{(m,e)}_{2,p2} M^{(m,m,e)}_{2,p2:2} \\ &= 1.025\,76(12), \\ M^{(e(m),e)}_{2,p4(p2)p2} &= 2M^{(e(m),e)}_{2,p4A(p2)p2} + 4M^{(e(m),e)}_{2,p4B(p2)p2} \\ &\quad - 4\Delta B^{(e,m)}_{2,p2} M^{(m,e,e)}_{2,p2:2} \\ &= 0.130\,84\,(2), \\ M^{(m(m),e)}_{2,p4(p2)p2} &= 2M^{(m(m),e)}_{2,p4A(p2)p2} + 4M^{(m(m),e)}_{2,p4B(p2)p2} \\ &\quad - 4\Delta B^{(m,m)}_{2,p2} M^{(m,m,e)}_{2,p2:2} \\ &= 7.173\,53\,(81) \times 10^{-2}, \\ M^{(e(e),m)}_{2,p4(p2)p2} &= 2M^{(e(e),m)}_{2,p4A(p2)p2} + 4M^{(e(e),m)}_{2,p4B(p2)p2} \\ &\quad - 4\Delta B^{(e,e)}_{2,p2} M^{(m,m,e)}_{2,p2:2} \\ &= 0.15845\,(3), \\ M^{(m(e),m)}_{2,p4(p2)p2} &= 2M^{(m(e),m)}_{2,p4A(p2)p2} + 4M^{(m(e),m)}_{2,p4B(p2)p2} \\ &\quad - 4\Delta B^{(m,e)}_{2,p2} M^{(m,m,m)}_{2,p2:2} \\ &= 4.826\,62\,(1) \times 10^{-2}, \\ M^{(e(m),m)}_{2,p4(p2)p2} &= 2M^{(e(m),m)}_{2,p4A(p2)p2} + 4M^{(e(m),m)}_{2,p4B(p2)p2} \\ &\quad - 4\Delta B^{(e,m)}_{2,p2} M^{(m,e,m)}_{2,p2:2} \\ &= 5.29020\,(63) \times 10^{-3}, \end{aligned} \tag{36, 37}$$

From these contributions we obtain $A_2[I(d)]$:

$$\begin{aligned} A_2[\mathrm{I}(d)] &= M^{(e(e),e)}_{2,p4(p2)p2} + M^{(m(e),e)}_{2,p4(p2)p2} + M^{(e(m),e)}_{2,p4(p2)p2} \\ &\quad + M^{(m(m),e)}_{2,p4(p2)p2} + M^{(e(e),m)}_{2,p4(p2)p2} + M^{(m(e),m)}_{2,p4(p2)p2} \\ &\quad + M^{(e(m),m)}_{2,p4(p2)p2} \\ &= 8.892\,07\,(102). \end{aligned} \tag{38}$$

Several terms of $A_2[\mathrm{I}(d)]$ was also evaluated by an alternative method using an exact spectral function of $\Pi_4(\Pi_2)$ in which two-loop masses are equal. They are listed at the bottom of Table II. They are in good agreement with the values given in (36) and (37).

$A_2[\mathrm{I}(e)]$ is evaluated using the Padé approximant for Π_6, which is known to be a very good approximation from an earlier work. Our result is

$$\begin{aligned} A_2[\mathrm{I}(e)] &= M^{(e,e)}_{2,p6p2} + M^{(e,m)}_{2,p6p2} + M^{(m,e)}_{2,p6p2} \\ &= -1.219\,20\,(71). \end{aligned} \tag{39}$$

$A_2[\mathrm{I}(f)]$ is evaluated using the entries of Table III together with Table VI. We obtain

$$\begin{aligned} a^{(m,e(e,e))}_{2,p4(p2:2)} &= \Delta M^{(m,e(e,e))}_{2,p4A(p2:2)} + \Delta M^{(m,e(e,e))}_{2,p4B(p2:2)} \\ &\quad - 2\Delta B^{(e(e,e))}_{2,p2:2} M^{(m,e)}_{2,p2} \\ &= 2.885\,98\,(9), \\ a^{(m,e(e,m))}_{2,p4(p2:2)} &= \Delta M^{(m,e(e,m))}_{2,p4A(p2:2)} + \Delta M^{(m,e(e,m))}_{2,p4B(p2:2)} \\ &\quad - 2\Delta B^{(e(e,m))}_{2,p2:2} M^{(m,e)}_{2,p2} \\ &= 0.161\,11\,(3), \\ a^{(m,e(m,m))}_{2,p4(p2:2)} &= \Delta M^{(m,e(m,m))}_{2,p4A(p2:2)} + \Delta M^{(m,e(m,m))}_{2,p4B(p2:2)} \\ &\quad - 2\Delta B^{(e(m,m))}_{2,p2:2} M^{(m,e)}_{2,p2} \\ &= 0.010\,63\,(1), \\ a^{(m,m(e,e))}_{2,p4(p2:2)} &= \Delta M^{(m,m(e,e))}_{2,p4A(p2:2)} + \Delta M^{(m,m(e,e))}_{2,p4B(p2:2)} \\ &\quad - 2\Delta B^{(m(e,e))}_{2,p2:2} M^{(m,m)}_{2,p2} \\ &= 0.53660(9), \\ a^{(m,m(e,m))}_{2,p4(p2:2)} &= \Delta M^{(m,m(e,m))}_{2,p4A(p2:2)} + \Delta M^{(m,m(e,m))}_{2,p4B(p2:2)} \\ &\quad - 2\Delta B^{(m(e,m))}_{2,p2:2} M^{(m,m)}_{2,p2} \\ &= 0.090\,79\,(2), \end{aligned} \tag{40}$$

From these contributions we obtain $A_2[\mathrm{I}(f)]$:

$$\begin{aligned} A_2[\mathrm{I}(f)] &= a^{(m,e(e,e))}_{2,p4(p2:2)} + a^{(m,e(e,m))}_{2,p4(p2:2)} + a^{(m,e(m,m))}_{2,p4(p2:2)} \\ &\quad + a^{(m,m(e,e))}_{2,p4(p2:2)} + a^{(m,m(e,m))}_{2,p4(p2:2)} \\ &= 3.685\,10\,(13). \end{aligned} \tag{41}$$

B. Set II

Integrals of Set II, except for subset II(e), can be readily obtained from eighth-order diagrams belonging to Group II by insertion of $\nu - p$ loops. We have evaluated only subsets II(a), II(b), and II(f) thus far. From Table IV and VI of this paper and Tables III and VI of [39], we obtain

TABLE IV. Numerical evaluation of Set II(a) which consists of II(a_1) and II(a_2). The Set II(a_1) has contributions denoted by Δ_1 and Set II(a_2) has contributions denoted by Δ_2. The symbol ()() indicates photon lines in which $\nu - p$ loops Π are inserted. n_F is the number of Feynman diagrams represented by the integral. Note that t.r. is time-reversed Feynman diagram.

Integral	n_F	Value (error) including n_F	Sampling per iteration	No. of iterations
$\Delta_1 M_{4a,p2:3}^{(e,e,e)()}$ + t.r.	6	15.156 11 (283)	1×10^8	160
$\Delta_1 M_{4a,p2:3}^{(e,e,m)()}$ + t.r.	18	1.317 96 (49)	1×10^8	200
$\Delta_1 M_{4a,p2:3}^{(e,m,m)()}$ + t.r.	18	0.091 09 (13)	1×10^8	100
$\Delta_1 M_{4a,p2:3}^{(m,m,m)()}$ + t.r.	6	0.004 13 (9)	1×10^7	20
$\Delta_1 M_{4b,p2:3}^{(e,e,e)()} + \Delta_1 M_{4b,p2:3}^{()(e,e,e)}$	6	−30.091 30 (191)	4×10^7	200
$\Delta_1 M_{4b,p2:3}^{(e,e,m)()} + \Delta_1 M_{4b,p2:3}^{()(e,e,m)}$	18	−6.381 88 (26)	1×10^8	100
$\Delta_1 M_{4b,p2:3}^{(e,m,m)()} + \Delta_1 M_{4b,p2:3}^{()(e,m,m)}$	18	−0.842 26 (4)	1×10^8	120
$\Delta_1 M_{4b,p2:3}^{(m,m,m)()} + \Delta_1 M_{4b,p2:3}^{()(m,m,m)}$	6	−0.054 22 (4)	1×10^7	20
$\Delta_2 M_{4a,p2:2,p2}^{(e,e)(e)}$ + t.r.	6	12.234 57 (99)	2×10^8	370
$\Delta_2 M_{4a,p2:2,p2}^{(e,e)(m)}$ + t.r.	6	0.019 71 (34)	1×10^7	120
$\Delta_2 M_{4a,p2:2,p2}^{(e,m)(e)}$ + t.r.	12	0.272 76 (35)	2×10^7	380
$\Delta_2 M_{4a,p2:2,p2}^{(m,m)(e)}$ + t.r.	6	−0.014 08 (27)	1×10^7	20
$\Delta_2 M_{4a,p2:2,p2}^{(e,m)(m)}$ + t.r.	12	−0.082 22 (22)	1×10^7	20
$\Delta_2 M_{4a,p2:2,p2}^{(m,m)(m)}$ + t.r.	6	−0.009 98 (3)	1×10^7	20
$\Delta_2 M_{4b,p2:2,p2}^{(e,e)(e)} + \Delta_2 M_{4b,p2,p2:2}^{(e)(e,e)}$	6	−28.69942 (79)	1×10^8	380
$\Delta_2 M_{4b,p2:2,p2}^{(e,e)(m)} + \Delta_2 M_{4b,p2,p2:2}^{(m)(e,e)}$	6	−1.720 76 (14)	1×10^7	100
$\Delta_2 M_{4b,p2:2,p2}^{(e,m)(e)} + \Delta_2 M_{4b,p2,p2:2}^{(e)(e,m)}$	12	−3.715 61 (32)	1×10^7	120
$\Delta_2 M_{4b,p2:2,p2}^{(m,m)(e)} + \Delta_2 M_{4b,p2,p2:2}^{(e)(m,m)}$	6	−0.239 56 (8)	1×10^7	20
$\Delta_2 M_{4b,p2:2,p2}^{(e,m)(m)} + \Delta_2 M_{4b,p2,p2:2}^{(m)(e,m)}$	12	−0.379 76 (7)	1×10^7	20
$\Delta_2 M_{4b,p2:2,p2}^{(m,m)(m)} + \Delta_2 M_{4b,p2,p2:2}^{(m)(m,m)}$	6	−0.036 19 (1)	1×10^7	20

$$
\begin{aligned}
M_{4,p2:3}^{(e,e,e)} &= 2M_{4a,p2:3}^{(e,e,e)} + M_{4b,p2:3}^{(e,e,e)\alpha} + M_{4b,p2:3}^{(e,e,e)\beta} \\
&\quad - \Delta B_2 M_{2,p2:3}^{(e,e,e)} - \Delta B_{2,p2:3}^{(e,e,e)} M_2 \\
&= -28.431\,32\,(344), \\
M_{4,p2:2,p2}^{(e,e)(e)} &= 2M_{4a,p2:2,p2}^{(e,e)(e)} + M_{4b,p2:2,p2}^{(e,e)(e)} + M_{4b,p2,p2:2}^{(e)(e,e)} \\
&\quad - \Delta B_{2,p2}^{(e)} M_{2,p2:2}^{(e,e)} - \Delta B_{2,p2:2}^{(e,e)} M_{2,p2}^{(e)} \\
&= -27.424\,32\,(127), \\
M_{4,p2:3}^{(e,e,m)} &= 2M_{4a,p2:3}^{(e,e,m)()} + M_{4b,p2:3}^{(e,e,m)()} + M_{4b,p2:3}^{()(e,e,m)} \\
&\quad - \Delta B_2 M_{2,p2:3}^{(e,e,m)} - \Delta B_{2,p2:3}^{(e,e,m)} M_2 \\
&= -6.792\,45\,(56), \\
M_{4,p2:2,p2}^{(e,e)(m)} &= 2M_{4a,p2:2,p2}^{(e,e)(m)} + M_{4b,p2:2,p2}^{(e,e)(m)} + M_{4b,p2,p2:2}^{(m)(e,e)} \\
&\quad - \Delta B_{2,p2}^{(m)} M_{2,p2:2}^{(e,e)} - \Delta B_{2,p2:2}^{(e,e)} M_{2,p2}^{(m)} \\
&= -1.957\,03\,(37),
\end{aligned}
\tag{42}
$$

$$
\begin{aligned}
M_{4,p2:2,p2}^{(e,m)(e)} &= 4M_{4a,p2:2,p2}^{(e,m)(e)} + 2M_{4b,p2:2,p2}^{(e,m)(e)} + 2M_{4b,p2,p2:2}^{(e)(e,m)} \\
&\quad - 2\Delta B_{2,p2}^{(e)} M_{2,p2:2}^{(e,m)} - 2\Delta B_{2,p2:2}^{(e,m)} M_{2,p2}^{(e)} \\
&= -4.148\,93\,(48), \\
M_{4,p2:3}^{(e,m,m)} &= 2M_{4a,p2:3}^{(e,m,m)} + M_{4b,p2:3}^{(e,m,m)()} + M_{4b,p2:3}^{()(e,m,m)} \\
&\quad - \Delta B_2 M_{2,p2:3}^{(e,m,m)} - \Delta B_{2,p2:3}^{(e,m,m)} M_2 \\
&= -0.952\,84\,(14), \\
M_{4,p2:2,p2}^{(m,m)(e)} &= 2M_{4a,p2:2,p2}^{(m,m)(e)} + M_{4b,p2:2,p2}^{(m,m)(e)} + M_{4b,p2,p2:2}^{(e)(m,m)} \\
&\quad - \Delta B_{2,p2}^{(e)} M_{2,p2:2}^{(m,m)} - \Delta B_{2,p2:2}^{(m,m)} M_{2,p2}^{(e)} \\
&= -0.289\,02\,(29), \\
M_{4,p2:2,p2}^{(e,m)(m)} &= 4M_{4a,p2:2,p2}^{(e,m)(m)} + 2M_{4b,p2:2,p2}^{(e,m)(m)} + 2M_{4b,p2,p2:2}^{(m)(e,m)} \\
&\quad - 2\Delta B_{2,p2}^{(m)} M_{2,p2:2}^{(e,m)} - 2\Delta B_{2,p2:2}^{(e,m)} M_{2,p2}^{(m)} \\
&= -0.475\,76\,(23).
\end{aligned}
\tag{43}
$$

Adding up these contributions one obtains

$$A_2[\mathrm{II}(a)] = -70.4717\,(38). \tag{44}$$

From Table V and VI of this paper and Tables III and VI of [39] we obtain

$$\begin{aligned}
M^{(e,e)}_{4,p4p2} &= 2\Delta_1 M^{(e,e)()}_{4a,p4p2} + \Delta_1 M^{(e,e)()}_{4b,p4p2} + \Delta_1 M^{()(e,e)}_{4b,p4p2} \\
&\quad + (p4 \leftrightarrow p2) - \Delta B_2 M^{(e,e)}_{2,p4p2} - \Delta B^{(e,e)}_{2,p4p2} M_2 \\
&= -19.041\,91\,(203), \\
M^{(e,m)}_{4,p4p2} &= 2\Delta_1 M^{(e,m)()}_{4a,p4p2} + \Delta_1 M^{(e,m)()}_{4b,p4p2} + \Delta_1 M^{()(e,m)}_{4b,p4p2} \\
&\quad + (p4 \leftrightarrow p2) - \Delta B_2 M^{(e,m)}_{2,p4p2} - \Delta B^{(e,m)}_{2,p4p2} M_2 \\
&= -1.288\,45\,(25), \\
M^{(m,e)}_{4,p4p2} &= 2\Delta_1 M^{(m,e)()}_{4a,p4p2} + \Delta_1 M^{(m,e)()}_{4b,p4p2} + \Delta_1 M^{()(m,e)}_{4b,p4p2} \\
&\quad + (p4 \leftrightarrow p2) - \Delta B_2 M^{(m,e)}_{2,p4p2} - \Delta B^{(m,e)}_{2,p4p2} M_2 \\
&= -3.131\,32\,(25),
\end{aligned} \tag{45}$$

$$\begin{aligned}
M^{(e)(e)}_{4,p4p2} &= 2\Delta_2 M^{(e)(e)}_{4a,p4p2} + \Delta_2 M^{(e)(e)}_{4b,p4p2} + (p4 \leftrightarrow p2) \\
&\quad - \Delta B^{(e)}_{2,p2} M^{(e)}_{2,p4} - \Delta B^{(e)}_{2,p4} M^{(e)}_{2,p2} \\
&= -9.426\,67\,(145), \\
M^{(e)(m)}_{4,p4p2} &= 2\Delta_2 M^{(e)(m)}_{4a,p4p2} + \Delta_2 M^{(e)(m)}_{4b,p4p2} + (p4 \leftrightarrow p2) \\
&\quad - \Delta B^{(m)}_{2,p2} M^{(e)}_{2,p4} - \Delta B^{(e)}_{2,p4} M^{(m)}_{2,p2} \\
&= -0.608\,77\,(18), \\
M^{(m)(e)}_{4,p4p2} &= 2\Delta_2 M^{(m)(e)}_{4a,p4p2} + \Delta_2 M^{(m)(e)}_{4b,p4p2} + (p4 \leftrightarrow p2) \\
&\quad - \Delta B^{(e)}_{2,p2} M^{(m)}_{2,p4} - \Delta B^{(m)}_{2,p4} M^{(e)}_{2,p2} \\
&= -1.274\,36\,(27).
\end{aligned} \tag{46}$$

Adding up these values we obtain

$$A_2[\mathrm{II}(b)] = -34.7715\,(26). \tag{47}$$

Table VII lists numerical results of set II(f) obtained in Version A. The results obtained by an alternate formulation (Version B) are listed in Table VIII. Combining the values in these tables statistically one obtains

TABLE V. Numerical evaluation of diagrams of Set II(b). Δ_1 indicates contributions in which Π's act on the same photon line while Δ_2 refers to those in which Π's act on different photon lines. The symbol ()() indicates photon lines in which $v - p$ loops Π are inserted. n_F is the number of Feynman diagrams represented by the integral. Note that t.r. is time-reversed Feynman diagram.

Integral	n_F	Value (error) including n_F	Sampling per iteration	No. of iterations
$\Delta_1 M^{(e,e)()}_{4a,p4p2} + (p4 \leftrightarrow p2) + \mathrm{t.r.}$	36	12.650 00 (135)	4×10^8	220
$\Delta_1 M^{(e,m)()}_{4a,p4p2} + (p4 \leftrightarrow p2) + \mathrm{t.r.}$	36	0.307 49 (22)	4×10^7	140
$\Delta_1 M^{(m,e)()}_{4a,p4p2} + (p4 \leftrightarrow p2) + \mathrm{t.r.}$	36	0.848 09 (23)	1×10^8	160
$\Delta_1 M^{(m,m)()}_{4a,p4p2} + (p4 \leftrightarrow p2) + \mathrm{t.r.}$	36	0.044 24 (33)	1×10^7	20
$\Delta_1 M^{(e,e)()}_{4b,p4p2} + \Delta_1 M^{()(e,e)}_{4b,p4p2} + (p4 \leftrightarrow p2)$	36	−19.707 81 (143)	1×10^8	220
$\Delta_1 M^{(e,m)()}_{4b,p4p2} + \Delta_1 M^{()(e,m)}_{4b,p4p2} + (p4 \leftrightarrow p2)$	36	−1.239 84 (10)	4×10^7	140
$\Delta_1 M^{(m,e)()}_{4b,p4p2} + \Delta_1 M^{()(m,e)}_{4b,p4p2} + (p4 \leftrightarrow p2)$	36	−3.069 74 (9)	1×10^8	200
$\Delta_1 M^{(m,m)()}_{4b,p4p2} + \Delta_1 M^{()(m,m)}_{4b,p4p2} + (p4 \leftrightarrow p2)$	36	−0.309 84 (15)	1×10^7	20
$\Delta_2 M^{(e)(e)}_{4a,p4p2} + \mathrm{t.r.}$	18	5.894 71 (107)	1×10^8	240
$\Delta_2 M^{(e)(m)}_{4a,p4p2} + \mathrm{t.r.}$	18	0.092 86 (16)	1×10^7	140
$\Delta_2 M^{(m)(e)}_{4a,p4p2} + \mathrm{t.r.}$	18	0.218 86 (23)	1×10^7	180
$\Delta_2 M^{(m)(m)}_{4a,p4p2} + \mathrm{t.r.}$	18	−0.017 23 (5)	1×10^7	20
$\Delta_2 M^{(e)(e)}_{4b,p4p2} + (p4 \leftrightarrow p2)$	18	−9.835 70 (97)	4×10^7	260
$\Delta_2 M^{(e)(m)}_{4b,p4p2} + (p4 \leftrightarrow p2)$	18	−0.568 67 (8)	1×10^7	120
$\Delta_2 M^{(m)(e)}_{4b,p4p2} + (p4 \leftrightarrow p2)$	18	−1.362 97 (13)	1×10^7	100
$\Delta_2 M^{(m)(m)}_{4b,p4p2} + (p4 \leftrightarrow p2)$	18	−0.107 56 (2)	1×10^7	20

TABLE VI. Numerical evaluation of diagrams for auxiliary quantities needed to evaluate contribution of Set I and Set II.

Integral	n_F	Value (error) including n_F	Sampling per iteration	No. of iterations
$\Delta B_{2,2:3}^{(e,e,e)}$	1	16.157 65 (75)	1×10^7	100
$\Delta B_{2,2:3}^{(e,e,m)}$	3	2.715 94 (12)	1×10^7	100
$\Delta B_{2,2:3}^{(e,m,m)}$	3	0.361 36 (4)	1×10^7	40
$\Delta B_{2,2:3}^{(m,m,m)}$	1	0.023 81 (1)	1×10^7	20
$\Delta B_{2,p4p2}^{(e,e)}$	6	13.276 21 (93)	1×10^7	100
$\Delta B_{2,p4p2}^{(e,m)}$	6	0.532 79 (5)	1×10^7	80
$\Delta B_{2,p4p2}^{(m,e)}$	6	1.318 84 (5)	1×10^7	120
$\Delta B_{2,p4p2}^{(m,m)}$	6	0.130 66 (2)	1×10^7	20
$\Delta B_{2,p2:2}^{(e(e,e))}$	1	0.027 91 (1)	1×10^6	40
$\Delta B_{2,p2:2}^{(m(e,e))}$	1	5.330 35 (20)	1×10^7	100
$\Delta B_{2,p2:2}^{(m(m,e))}$	2	0.472 08 (9)	1×10^6	40
$\Delta B_{2,p2:2}^{(e(m,e))}$	2	$3.6159\,(8) \times 10^{-5}$	1×10^6	40
$\Delta B_{2,p2:2}^{(e(m,m))}$	1	$8.3020\,(36) \times 10^{-7}$	1×10^6	20

$$
\begin{aligned}
A_2[\mathrm{II}(f)]^{(e,e)} &= -57.0633\,(109),\\
A_2[\mathrm{II}(f)]^{(e,m)} &= -4.7157\,(31),\\
A_2[\mathrm{II}(f)]^{(m,e)} &= -15.6857\,(37).
\end{aligned}
\tag{48}
$$

From (48) one obtains

$$
A_2[\mathrm{II}(f)] = -77.4648\,(120). \tag{49}
$$

TABLE VII. Numerical evaluation of diagrams of Set II(f) in Version A. The suffix p indicates insertion of Π_2 in the photon lines connecting the muon line and the $l-l$ loop. $A_2[2f]^{(x,y)} \equiv \Delta M_{8LLJp}^{(x,y)} + \Delta M_{8LLKp}^{(x,y)} + \Delta M_{8LLLp}^{(x,y)}$. $r = \Delta M_{8LLxp}/\Delta M_{8LLx}$, where $x = J, K, L$, in column 6 is for comparison with the enhancement factor $4K_\eta$ for Set II(f) discussed in Sec. III. The logarithmic enhancement comes from the $v-p$ loop only. This is consistent with $r \simeq 11 \sim 15$ for (e,e), (me) and $r \simeq 0.7 \sim 2$ for (e,m), (m,m).

Integral	n_F	Value (error) including n_F	Sampling per iteration	No. of iterations	r
$\Delta M_{8LLJp}^{(e,e)}$	24	70.6567 (254)	4×10^7	220	11.05
$\Delta M_{8LLJp}^{(m,e)}$	24	35.0760 (78)	2×10^7	200	13.74
$\Delta M_{8LLJp}^{(e,m)}$	24	6.0056 (26)	2×10^7	200	0.94
$\Delta M_{8LLJp}^{(m,m)}$	24	3.7717 (17)	1×10^7	140	1.48
$\Delta M_{8LLKp}^{(e,e)}$	24	−87.8367 (291)	8×10^7	210	11.29
$\Delta M_{8LLKp}^{(m,e)}$	24	−26.1793 (83)	2×10^7	220	13.97
$\Delta M_{8LLKp}^{(e,m)}$	24	−5.4760 (29)	2×10^7	230	0.70
$\Delta M_{8LLKp}^{(m,m)}$	24	−2.9311 (17)	1×10^7	140	1.56
$\Delta M_{8LLLp}^{(e,e)}$	24	−39.9514 (287)	4×10^7	310	13.07
$\Delta M_{8LLLp}^{(m,e)}$	24	−24.5877 (81)	2×10^7	220	14.73
$\Delta M_{8LLLp}^{(e,m)}$	24	−5.2468 (29)	2×10^7	200	1.71
$\Delta M_{8LLLp}^{(m,m)}$	24	−3.2771 (17)	1×10^7	140	1.96
$A_2[2f]^{(e,e)}$	72	−57.1314 (481)			
$A_2[2f]^{(m,e)}$	72	−15.6910 (140)			
$A_2[2f]^{(e,m)}$	72	−4.7172 (49)			
$A_2[2f]^{(m,m)}$	72	−2.4365 (29)			

TABLE VIII. Numerical evaluation of diagrams of Set II(f) in Version B. The symbol p indicates insertion of Π_2 in the photon lines connecting the muon line and the light–light loop. $JKLp^{(x,y)} \equiv \Delta M^{(x,y)}_{8LLJp} + \Delta M^{(x,y)}_{8LLKp} + \Delta M^{(x,y)}_{8LLLp}$. The suffix 2 or 13 below indicates the muon line into which the magnetic field vertex is inserted. $A_2[2f]^{(x,y)} \equiv JKLp_2^{(x,y)} + JKLp_{13}^{(x,y)}$. $r = JKLp/JKL$ in column 6 is for comparison with the enhancement factor $4K_\eta$ for Set II(f) discussed in Sec. III.

Integral	n_F	Value (error) including n_F	Sampling per iteration	No. of iterations	r
$JKLp_2^{(e,e)}$	24	−11.377 74 (313)	1×10^7, 1×10^9	250, 20	12.35
$JKLp_2^{(m,e)}$	24	−1.871 16 (30)	1×10^7	250	15.86
$JKLp_2^{(e,m)}$	24	−0.749 46 (64)	1×10^7	250	0.81
$JKLp_2^{(m,m)}$	24	−0.280 35 (39)	1×10^7	250	2.38
$JKLp_{13}^{(e,e)}$	48	−45.681 88 (1079)	1×10^8, 1×10^9	450, 100	13.03
$JKLp_{13}^{(m,e)}$	48	−13.814 20 (386)	1×10^7, 1×10^9	250, 40	15.82
$JKLp_{13}^{(e,m)}$	48	−3.965 27 (399)	1×10^7	250	1.13
$JKLp_{13}^{(m,m)}$	48	−2.153 39 (182)	1×10^7	250	2.47
$A_2[2f]^{(e,e)}$	72	−57.0596 (113)			
$A_2[2f]^{(m,e)}$	72	−15.6854 (39)			
$A_2[2f]^{(e,m)}$	72	−4.7147 (40)			
$A_2[2f]^{(m,m)}$	72	−2.4338 (19)			

C. Set VI

By far the largest contribution to $A_2^{(10)}$ comes from the subset VI(a), followed by the subset VI(b). Their integrals can be readily obtained by insertion of $\nu - p$ functions Π_2 and Π_4 into the sixth-order diagram M_{6LL}. We have evaluated them precisely by VEGAS. The results are listed in Table IX. Summing them up, we obtain

$$A_2[\mathrm{VI}(a)] = 629.1407\,(118), \tag{50}$$

and

$$A_2[\mathrm{VI}(b)] = 181.1285\,(51). \tag{51}$$

The difference between VI(a)[e,e,e] of Table IX and the old one in Eq. (2.49) of [42] is due to a program error in the latter. The results in Table IX show that the leading term estimate (24) is an overestimate by a factor two, while the estimate (25) is not too far off.

Contributions of subsets VI(c), VI(e), VI(f), and VI(i) are also not difficult to evaluate, since they can be readily obtained by insertion of Π_2 into some eighth-order integrals. Their numerical values are listed in Tables X, XI, XII, and XIII. From this we obtain

TABLE IX. Numerical evaluation of diagrams of Set VI(a) and Set VI(b). The notation follows that of [42] with some modification and adaptation.

Integral	n_F	Value (error) including n_F	Sampling per iteration	No. of iterations
$M^{(e,e,e)}_{6LL,p2p2}$	6	542.911 80 (910)	1×10^9	300
$M^{(e,e,m)}_{6LL,p2p2}$	72	39.003 49 (272)	1×10^8	200
$M^{(e,m,m)}_{6LL,p2p2}$	36	2.430 29 (22)	1×10^8	200
$M^{(m,e,e)}_{6LL,p2p2}$	36	34.423 89 (680)	1×10^8	200
$M^{(m,e,m)}_{6LL,p2p2}$	72	10.371 25 (162)	1×10^8	200
$M^{(m,m,m)}_{6LL,p2p2}$	36	1.041 71 (37)	1×10^8	20
$M^{(e,e)}_{6LL,p4}$	54	168.728 55 (478)	1×10^9	200
$M^{(e,m)}_{6LL,p4}$	54	7.583 83 (50)	1×10^8	210
$M^{(m,e)}_{6LL,p4}$	54	4.816 14 (164)	1×10^8	200
$M^{(m,m)}_{6LL,p4}$	54	1.347 26 (30)	1×10^8	140

TABLE X. Numerical evaluation of diagrams of Set VI(c). The notation follows that of [42] with some modification and adaptation. The suffix p indicates insertion of Π_2 in the photon lines connecting the muon line and $l-l$ loop. $r = \Delta M_{8LLxp}/\Delta M_{8LLx}$, where $x = E, F, G, H, I$, in column 6 is for comparison with the crude enhancement factor $3K_\eta$ for Set VI(c) discussed in Sec. III.

Integral	n_F	Value (error) including n_F	Sampling per iteration	No. of iterations	r
$\Delta M^{(e,e)}_{8LLEp}$	18	−82.9940 (141)	2×10^8	200	3.84
$\Delta M^{(e,m)}_{8LLEp}$	18	−1.8277 (18)	1×10^7	40	
$\Delta M^{(m,e)}_{8LLEp}$	18	−3.3463 (44)	1×10^7	140	
$\Delta M^{(m,m)}_{8LLEp}$	18	−0.6168 (6)	1×10^7	140	
$\Delta M^{(e,e)}_{8LLFp}$	36	−322.4493 (573)	2×10^8	280	4.25
$\Delta M^{(e,m)}_{8LLFp}$	36	−5.2571 (60)	1×10^7	80	
$\Delta M^{(m,e)}_{8LLFp}$	36	−9.3199 (64)	4×10^7	390	
$\Delta M^{(m,m)}_{8LLFp}$	36	−1.5392 (17)	1×10^7	280	
$\Delta M^{(e,e)}_{8LLGp}$	36	−181.5345 (489)	2×10^8	210	5.17
$\Delta M^{(e,m)}_{8LLGp}$	36	−3.3841 (61)	1×10^7	80	
$\Delta M^{(m,e)}_{8LLGp}$	36	−6.5157 (84)	4×10^7	300	
$\Delta M^{(m,m)}_{8LLGp}$	36	−0.9499 (18)	1×10^7	300	
$\Delta M^{(e,e)}_{8LLHp}$	18	230.3344 (590)	4×10^8	400	4.27
$\Delta M^{(e,m)}_{8LLHp}$	18	2.2093 (74)	1×10^7	66	
$\Delta M^{(m,e)}_{8LLHp}$	18	2.1519 (96)	4×10^7	480	
$\Delta M^{(m,m)}_{8LLHp}$	18	0.2839 (18)	1×10^7	320	
$\Delta M^{(e,e)}_{8LLIp}$	36	514.7317 (567)	2×10^8	300	4.57
$\Delta M^{(e,m)}_{8LLIp}$	36	7.0544 (59)	1×10^7	80	
$\Delta M^{(m,e)}_{8LLIp}$	36	9.2489 (68)	4×10^7	320	
$\Delta M^{(m,m)}_{8LLIp}$	36	1.1912 (13)	1×10^7	340	

$$
\begin{aligned}
A_2[\mathrm{VI}(c)]^{(e,e)} &= \Delta M^{(e,e)}_{8LLEp} + \Delta M^{(e,e)}_{8LLFp} + \Delta M^{(e,e)}_{8LLGp} \\
&\quad + \Delta M^{(e,e)}_{8LLHp} + \Delta M^{(e,e)}_{8LLIp} - 2\Delta B_2 M^{(e,e)}_{6LLp} \\
&= -17.0505\,(1122), \\
A_2[\mathrm{VI}(c)]^{(m,e)} &= \Delta M^{(m,e)}_{8LLEp} + \Delta M^{(m,e)}_{8LLFp} + \Delta M^{(m,e)}_{8LLGp} \\
&\quad + \Delta M^{(m,e)}_{8LLHp} + \Delta M^{(m,e)}_{8LLIp} - 2\Delta B_2 M^{(m,e)}_{6LLp} \\
&= -14.2744\,(105), \\
A_2[\mathrm{VI}(c)]^{(e,m)} &= \Delta M^{(e,m)}_{8LLEp} + \Delta M^{(e,m)}_{8LLFp} + \Delta M^{(e,m)}_{8LLGp} \\
&\quad + \Delta M^{(e,m)}_{8LLHp} + \Delta M^{(e,m)}_{8LLIp} - 2\Delta B_2 M^{(e,m)}_{6LLp} \\
&= -5.2514\,(129), \\
A_2[\mathrm{VI}(c)] &= A_2[\mathrm{VI}(c)]^{(e,e)} + A_2[\mathrm{VI}(c)]^{(m,e)} \\
&\quad + A_2[\mathrm{VI}(c)]^{(e,m)} \\
&= -36.5763\,(1141),
\end{aligned}
\tag{52}
$$

$$
\begin{aligned}
A_2[\mathrm{VI}(e)]^{(e,e)} &= \Delta M^{(e,e)}_{8LLEq} + \Delta M^{(e,e)}_{8LLFq} + \Delta M^{(e,e)}_{8LLGq} \\
&\quad + \Delta M^{(e,e)}_{8LLHq} + \Delta M^{(e,e)}_{8LLIq} - 2\Delta B^{(m,e)}_{2,p2} M_{6LL} \\
&= 0.7524\,(1338), \\
A_2[\mathrm{VI}(e)]^{(m,e)} &= \Delta M^{(m,e)}_{8LLEq} + \Delta M^{(m,e)}_{8LLFq} + \Delta M^{(m,e)}_{8LLGq} \\
&\quad + \Delta M^{(m,e)}_{8LLHq} + \Delta M^{(m,e)}_{8LLIq} - 2\Delta B^{(m,e)}_{2,p2} M^{(m,m)}_{6LL} \\
&= -3.9789\,(78), \\
A_2[\mathrm{VI}(e)]^{(e,m)} &= \Delta M^{(e,m)}_{8LLEq} + \Delta M^{(e,m)}_{8LLFq} + \Delta M^{(e,m)}_{8LLGq} \\
&\quad + \Delta M^{(e,m)}_{8LLHq} + \Delta M^{(e,m)}_{8LLIq} - 2\Delta B^{(m,m)}_{2,p2} M_{6LL} \\
&= -1.0950\,(35), \\
A_2[\mathrm{VI}(e)] &= A_2[\mathrm{VI}(e)]^{(e,e)} + A_2[\mathrm{VI}(e)]^{(m,e)} \\
&\quad + A_2[\mathrm{VI}(e)]^{(e,m)} \\
&= -4.3215\,(1341),
\end{aligned}
\tag{53}
$$

TABLE XI. Numerical evaluation of diagrams of Set VI(e). The notation follows that of [42] with some modification and adaptation. The suffix q refers to insertion of Π_2 in radiative corrections to the muon line. $r = \Delta M_{8LLxp}/\Delta M_{8LLx}$, where $x = E, F, G, H, I$, in column 6 is for comparison with the crude enhancement factor for Set VI(e) discussed in Sec. III.

Integral	n_F	Value (error) including n_F	Sampling per iteration	No. of iterations	r
$\Delta M^{(e,e)}_{8LLEq}$	6	$-35.1438\,(514)$	1×10^7	80	1.62
$\Delta M^{(e,m)}_{8LLEq}$	6	$0.0505\,(16)$	1×10^7	40	
$\Delta M^{(m,e)}_{8LLEq}$	6	$-0.9986\,(17)$	1×10^7	120	
$\Delta M^{(m,m)}_{8LLEq}$	6	$-0.1347\,(2)$	1×10^7	80	
$\Delta M^{(e,e)}_{8LLFq}$	12	$-100.5201\,(458)$	4×10^7	220	1.33
$\Delta M^{(e,m)}_{8LLFq}$	12	$0.3570\,(19)$	1×10^7	100	
$\Delta M^{(m,e)}_{8LLFq}$	12	$-2.4368\,(41)$	1×10^7	140	
$\Delta M^{(m,m)}_{8LLFq}$	12	$-0.2254\,(3)$	1×10^7	100	
$\Delta M^{(e,e)}_{8LLGq}$	12	$-38.1520\,(399)$	1×10^7	80	1.09
$\Delta M^{(e,m)}_{8LLGq}$	12	$-0.2662\,(7)$	1×10^7	40	
$\Delta M^{(m,e)}_{8LLGq}$	12	$-1.6144\,(33)$	1×10^7	180	
$\Delta M^{(m,m)}_{8LLGq}$	12	$-0.0957\,(3)$	1×10^7	80	
$\Delta M^{(e,e)}_{8LLHq}$	6	$64.5209\,(879)$	1×10^7	80	1.19
$\Delta M^{(e,m)}_{8LLHq}$	6	$-0.4527\,(12)$	1×10^7	40	
$\Delta M^{(m,e)}_{8LLHq}$	6	$0.3954\,(39)$	1×10^7	160	
$\Delta M^{(m,m)}_{8LLHq}$	6	$-0.221\,(91)\times10^{-3}$	1×10^7	80	
$\Delta M^{(e,e)}_{8LLIq}$	12	$189.0518\,(620)$	4×10^7	200	1.68
$\Delta M^{(e,m)}_{8LLIq}$	12	$1.8726\,(19)$	1×10^7	80	
$\Delta M^{(m,e)}_{8LLIq}$	12	$2.0747\,(37)$	1×10^7	200	
$\Delta M^{(m,m)}_{8LLIq}$	12	$0.0719\,(2)$	1×10^7	80	

$$
\begin{aligned}
A_2[\mathrm{VI}(f)]^{(e,e)} &= \Delta M^{(e,e)}_{8LLAp} + \Delta M^{(e,e)}_{8LLBp} + \Delta M^{(e,e)}_{8LLCp} \\
&\quad + \Delta M^{(e,e)}_{8LLDp} - 3\Delta B_2 M^{(e,e)}_{6LLp} \\
&= -45.0425\,(1463), \\
A_2[\mathrm{VI}(f)]^{(m,e)} &= \Delta M^{(m,e)}_{8LLAp} + \Delta M^{(m,e)}_{8LLBp} + \Delta M^{(m,e)}_{8LLCp} \\
&\quad + \Delta M^{(m,e)}_{8LLDp} - 3\Delta B_2 M^{(m,e)}_{6LLp} \\
&= 8.7673\,(228), \\
A_2[\mathrm{VI}(f)]^{(e,m)} &= \Delta M^{(e,m)}_{8LLAp} + \Delta M^{(e,m)}_{8LLBp} + \Delta M^{(e,m)}_{8LLCp} \\
&\quad + \Delta M^{(e,m)}_{8LLDp} - 3\Delta B_2 M^{(e,m)}_{6LLp} \\
&= -1.8847\,(155), \\
A_2[\mathrm{VI}(f)] &= A_2[\mathrm{VI}(f)]^{(e,e)} + A_2[\mathrm{VI}(f)]^{(m,e)} \\
&\quad + A_2[\mathrm{VI}(f)]^{(e,m)} \\
&= -38.1598\,(1488),
\end{aligned}
\tag{54}
$$

$$
\begin{aligned}
A_2[\mathrm{VI}(i)]^{(e,e)} &= \Delta M^{(e,e)}_{8LLAq} + \Delta M^{(e,e)}_{8LLBq} + \Delta M^{(e,e)}_{8LLCq} \\
&\quad + \Delta M^{(e,e)}_{8LLDq} - 3\Delta B^{(e,e)}_{2,p2} M_{6LL} \\
&= -28.3367\,(1142), \\
A_2[\mathrm{VI}(i)]^{(m,e)} &= \Delta M^{(m,e)}_{8LLAq} + \Delta M^{(m,e)}_{8LLBq} + \Delta M^{(m,e)}_{8LLCq} \\
&\quad + \Delta M^{(m,e)}_{8LLDq} - 3\Delta B^{(m,e)}_{2,p2} M^{(m,m)}_{6LL} \\
&= 2.0977\,(105), \\
A_2[\mathrm{VI}(i)]^{(e,m)} &= \Delta M^{(e,m)}_{8LLAq} + \Delta M^{(e,m)}_{8LLBq} + \Delta M^{(e,m)}_{8LLCq} \\
&\quad + \Delta M^{(e,m)}_{8LLDq} - 3\Delta B^{(e,m)}_{2,p2} M_{6LL} \\
&= -1.0983\,(31), \\
A_2[\mathrm{VI}(i)] &= A_2[\mathrm{VI}(i)]^{(e,e)} + A_2[\mathrm{VI}(i)]^{(m,e)} \\
&\quad + A_2[\mathrm{VI}(i)]^{(e,m)} \\
&= -27.3373\,(1147).
\end{aligned}
\tag{55}
$$

TABLE XII. Numerical evaluation of diagrams of Set VI(f). The notation follows that of [42] with some modification and adaptation. The suffix p indicates insertion of Π_2 in the photon lines connecting the muon line and the $l-l$ loop. $r = \Delta M_{8LLxp}/\Delta M_{8LLx}$, where $x = A, B, C, D$, in column 6 is for comparison with the enhancement factor $3K_\eta$ for Set VI(f) discussed in Sec. III.

Integral	n_F	Value (error) including n_F	Sampling per iteration	No. of iterations	r
$\Delta M^{(e,e)}_{8LLAp}$	30	307.3206 (848)	4×10^7	200	5.90
$\Delta M^{(e,m)}_{8LLAp}$	30	8.9175 (82)	1×10^7	120	
$\Delta M^{(m,e)}_{8LLAp}$	30	2.9097 (118)	1×10^7	100	
$\Delta M^{(m,m)}_{8LLAp}$	30	0.7878 (10)	1×10^7	200	
$\Delta M^{(e,e)}_{8LLBp}$	60	−482.5729 (603)	1×10^8	200	6.43
$\Delta M^{(e,m)}_{8LLBp}$	60	−16.0636 (78)	1×10^7	120	
$\Delta M^{(m,e)}_{8LLBp}$	60	−13.7242 (121)	2×10^7	100	
$\Delta M^{(m,m)}_{8LLBp}$	60	−1.7449 (12)	1×10^7	280	
$\Delta M^{(e,e)}_{8LLCp}$	60	645.3472 (823)	1×10^8	200	6.00
$\Delta M^{(e,m)}_{8LLCp}$	60	19.7833 (82)	1×10^7	180	
$\Delta M^{(m,e)}_{8LLCp}$	60	30.4954 (125)	2×10^7	240	
$\Delta M^{(m,m)}_{8LLCp}$	60	3.4824 (16)	1×10^7	300	
$\Delta M^{(e,e)}_{8LLDp}$	30	−252.4292(616)	4×10^7	200	6.67
$\Delta M^{(e,m)}_{8LLDp}$	30	−8.4527(66)	1×10^7	80	
$\Delta M^{(m,e)}_{8LLDp}$	30	−1.1736(86)	1×10^7	140	
$\Delta M^{(m,m)}_{8LLDp}$	30	−0.4074(8)	1×10^7	200	

TABLE XIII. Numerical evaluation of diagrams of Set VI(i). The notation follows that of [42] with some modification and adaptation. The suffix q refers to insertion of Π_2 in radiative corrections to the $l-l$ loop. $r = \Delta M_{8LLxp}/\Delta M_{8LLx}$, where $x = A, B, C, D$, in column 6 is for comparison with the enhancement factor K_η for Set VI(i) discussed in Sec. III.

Integral	n_F	Value (error) including n_F	Sampling per iteration	No. of iterations	r
$\Delta M^{(e,e)}_{8LLAq}$	10	29.6915 (199)	1×10^7	80	0.57
$\Delta M^{(e,m)}_{8LLAq}$	10	0.0914 (3)	1×10^7	40	
$\Delta M^{(m,e)}_{8LLAq}$	10	0.4867 (30)	1×10^7	100	
$\Delta M^{(m,m)}_{8LLAq}$	10	$0.8068\,(93) \times 10^{-2}$	1×10^7	140	
$\Delta M^{(e,e)}_{8LLBq}$	20	−81.3369 (946)	1×10^7	95*	1.08
$\Delta M^{(e,m)}_{8LLBq}$	20	−1.2816 (26)	1×10^7	100	
$\Delta M^{(m,e)}_{8LLBq}$	20	−4.6043 (69)	1×10^7	138	
$\Delta M^{(m,m)}_{8LLBq}$	20	−0.4926 (8)	1×10^7	200	
$\Delta M^{(e,e)}_{8LLCq}$	20	71.0664 (409)	1×10^7	80	0.66
$\Delta M^{(e,m)}_{8LLCq}$	20	0.7624 (7)	1×10^7	40	
$\Delta M^{(m,e)}_{8LLCq}$	20	8.5729 (59)	1×10^7	160	
$\Delta M^{(m,m)}_{8LLCq}$	20	0.5564 (4)	1×10^7	100	
$\Delta M^{(e,e)}_{8LLDq}$	10	−43.7735 (449)	1×10^7	80	1.16
$\Delta M^{(e,m)}_{8LLDq}$	10	−0.6699 (14)	1×10^7	60	
$\Delta M^{(m,e)}_{8LLDq}$	10	−0.2587 (42)	1×10^7	100	
$\Delta M^{(m,m)}_{8LLDq}$	10	−0.0551 (5)	1×10^7	140	

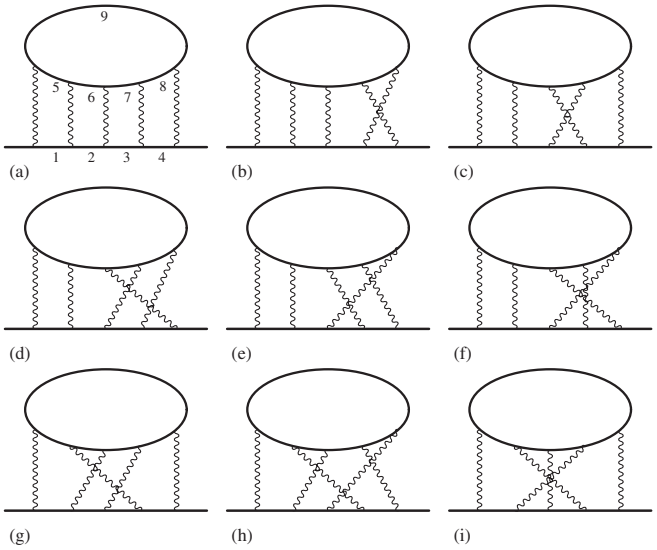

FIG. 7. Subset VI[k].

The last columns of Table X and XII show that the factor r is roughly equal to $3K_\eta$ with $K_\eta \simeq 2$ for sets VI(c) and VI(f). These factors vary from diagram to diagram within each set, making naive estimates for the sums of diagrams given in (27) entirely different from the corresponding terms of (52)–(55) and (27) obtained by explicit numerical integration. The ''enhancement'' factor is $K_\eta \sim 1$ for Sets VI(e) and VI(i). Table XI and Table XIII show that $K_\eta \sim 1$ in these cases, indicating that there is no significant enhancement. This is probably because Π_2 is buried deep in other subdiagrams in these cases.

Among the remaining subsets the subset VI(k) is likely to be the largest and most challenging because it has a subdiagram Λ_6 which consists of 120 proper lepton loops to which six photon lines are attached. See Fig. 7. This is a diagram which appears for the first time in the tenth-order so that it cannot be derived from or related to lower-order diagrams.

Another point of interest is that its leading logarithmic term is known (29) and was used to estimate its contribution to $a_\mu^{(10)}$. However, to determine the actual contribution of VI(k) we must find the nonleading term, too. To answer this question it is best to evaluate VI(k) explicitly.

It turns out that this is not difficult. Our first step is to reduce the number of independent integrals to 12 using the Ward-Takahashi identity, and reduce it further to 9 using the time-reversal symmetry.[1] Each integral generated by FORM has more than 90 000 terms occupying about 30 000 lines of FORTRAN code. This is certainly huge, but not unmanageable since it is only 30 times larger than typical eighth-order integrals. We also note that this subset is particularly simple in the sense that it is entirely free from UV- and IR-divergences. Numerical integration over 13-dimensional Feynman parameter space can be handled without difficulty by VEGAS. The result of numerical integration is listed in Table XV, from which we obtain

$$A_2[\mathrm{VI}(k)] = 97.123\,(62). \tag{56}$$

Clearly the previous estimate was an overestimate by about 100.

Another possibly large term is VI(j) [162 vertex diagrams] which we decided to evaluate explicitly. See Fig. 8. With the help of Ward-Takahashi identity and time-reversal invariance it can be represented by four independent integrals. FORM generated about 42 000 terms for each integral occupying about 18 000 lines of FORTRAN code. The result of numerical integration is listed in Table XIV, from which we obtain

$$A_2[\mathrm{VI}(j)] = -25.505\,(20). \tag{57}$$

The subsets yet to be evaluated are VI(d), VI(g), and VI(h). We foresee no technical problem in dealing with these subsets.

Some results described in this section can be compared with the results obtained by the renormalization group method. See [49] for details.

VI. CONTRIBUTION TO ELECTRON $g-2$

All tables also contain values of mass-independent contributions from 958 vertex diagrams belonging to 17 gauge-invariant subsets. These are actually contributions to $A_1^{(10)}$, namely, the electron $g-2$. Their values, including residual renormalization terms whenever they are required, are listed below:

$$\begin{aligned}
A_1[\mathrm{I}(a)] &= 4.7094\,(6) \times 10^{-4},\\
A_1[\mathrm{I}(b)] &= 7.0108\,(7) \times 10^{-3},\\
A_1[\mathrm{I}(c)] &= 2.3468\,(2) \times 10^{-2},\\
A_1[\mathrm{I}(d)] &= 4.4517(5) \times 10^{-3},\\
A_1[\mathrm{I}(e)] &= 1.0296(4) \times 10^{-2},\\
A_1[\mathrm{I}(f)] &= 8.4459\,(14) \times 10^{-3}.
\end{aligned} \tag{58}$$

[1]We noticed that $X6k_f$ is actually identical with $X6k_b$ while checking the proof. Thus the number of independent integrals of set VI is 8, not 9. Fortunately this does not affect our numerical result given in Eq. (56).

TABLE XIV. Numerical evaluation of diagrams of Set VI(j) contributing to the muon $g-2$. In the superscript (a, b), a and b refer to the external and internal light-by-light-scattering loop, respectively. Last 4 lines with superscript (m, m) are mass-independent so that they are identical with the contributions to the electron $g-2$.

Integral	n_F	Value (Error) including n_F	Sampling per iteration	No. of iterations
$X6j_a^{(e,e)}$	24	0.579 28 (0.013 86)	1×10^8,1×10^9	100, 294
$X6j_b^{(e,e)}$	12	−16.912 35 (0.006 30)	1×10^8,1×10^9	100, 100
$X6j_c^{(e,e)}$	12	−23.008 01 (0.00777)	1×10^8,1×10^9	100, 160
$X6j_d^{(e,e)}$	6	15.381 81 (0.003 88)	1×10^8,1×10^9	100, 87
$X6j_a^{(e,m)}$	24	4.752 11 (0.006 09)	1×10^8	105
$X6j_b^{(e,m)}$	12	−0.845 70 (0.001 12)	1×10^8	100
$X6j_c^{(e,m)}$	12	−5.963 39 (0.001 57)	1×10^8	190
$X6j_d^{(e,m)}$	6	0.881 53 (0.000 46)	1×10^8	220
$X6j_a^{(m,e)}$	24	−2.069 21 (0.005 49)	1×10^8	100
$X6j_b^{(m,e)}$	12	−3.752 00 (0.00232)	1×10^8	100
$X6j_c^{(m,e)}$	12	1.644 53 (0.00162)	1×10^8	200
$X6j_d^{(m,e)}$	6	3.806 56 (0.001 38)	1×10^8	130
$X6j_a^{(m,m)}$	24	−0.226 01 (0.001 43)	1×10^8	180
$X6j_b^{(m,m)}$	12	−0.696 98 (0.000 65)	1×10^8	100
$X6j_c^{(m,m)}$	12	−0.027 53 (0.000 53)	1×10^8	170
$X6j_d^{(m,m)}$	6	0.721 70 (0.000 37)	1×10^8	100

TABLE XV. Numerical evaluation of diagrams of Set VI(k) contributing to the muon $g-2$. The superscript e (m) indicates that the lepton loop Λ_6 is the electron (muon) loop. The latter is mass-independent so that it is identical with the contribution to the electron $g-2$.

Integral	n_F	Value (Error) including n_F	Sampling per iteration	No. of iterations
$X6k_a^{(e)}$	10	50.359 21 (0.01998)	1×10^8, 1×10^9	500, 150
$X6k_b^{(,e)}$	10	1.726 69 (0.017 86)	1×10^8	400
$X6k_c^{(e)}$	20	7.813 30 (0.020 38)	1×10^8	300
$X6k_d^{(e)}$	20	20.678 40 (0.037 58)	1×10^8	100
$X6k_e^{(e)}$	10	−0.194 66 (0.010 45)	1×10^8	300
$X6k_f^{(e)}$	10	1.758 90 (0.023 74)	1×10^8	230
$X6k_g^{(e)}$	20	−0.026 07 (0.01797)	1×10^8	200
$X6k_h^{(e)}$	10	−0.690 54 (0.007 50)	1×10^8	100
$X6k_i^{(e)}$	10	15.697 36 (0.015 95)	1×10^8	200
$X6k_a^{(m)}$	10	−0.560 22 (0.003 01)	1×10^8	100
$X6k_b^{(m)}$	10	0.302 82 (0.000 85)	1×10^8	100
$X6k_c^{(m)}$	20	−0.325 47 (0.001 14)	1×10^8	100
$X6k_d^{(m)}$	20	0.823 80 (0.000 84)	1×10^8	100
$X6k_e^{(m)}$	10	−0.171 88 (0.000 53)	1×10^8	100
$X6k_f^{(m)}$	10	0.303 29 (0.000 88)	1×10^8	100
$X6k_g^{(m)}$	20	−0.948 43 (0.00067)	1×10^8	100
$X6k_h^{(m)}$	10	−0.138 77 (0.000 18)	1×10^8	100
$X6k_i^{(m)}$	10	1.395 10 (0.000 69)	1×10^8	100

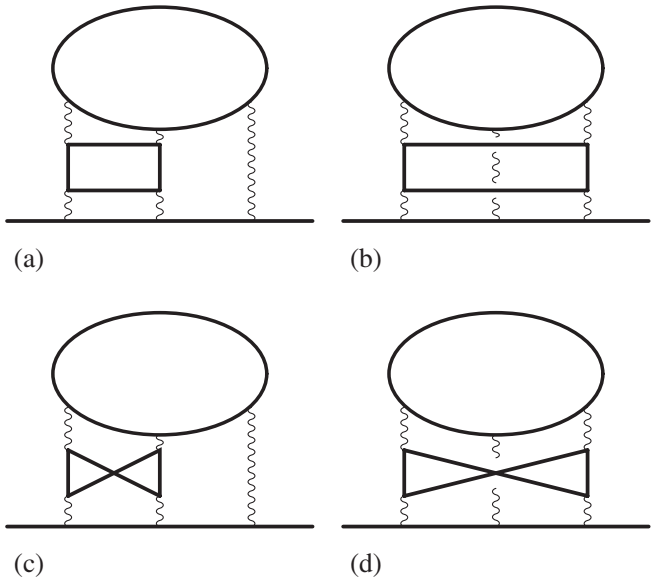

FIG. 8. Subset VI[j].

$$A_1[\mathrm{II}(a)] = 4.130(90) \times 10^{-3},$$
$$A_1[\mathrm{II}(b)] = -5.422(4) \times 10^{-2}, \quad (59)$$
$$A_1[\mathrm{II}(f)] = -2.434(2).$$

$$A_1[\mathrm{VI}(a)] = 1.0417\,(4),$$
$$A_1[\mathrm{VI}(b)] = 1.3473\,(3),$$
$$A_1[\mathrm{VI}(c)] = -2.5922\,(34),$$
$$A_1[\mathrm{VI}(e)] = -0.4312\,(6),$$
$$A_1[\mathrm{VI}(f)] = 0.7703\,(24), \quad (60)$$
$$A_1[\mathrm{VI}(i)] = -0.0438\,(11),$$
$$A_1[\mathrm{VI}(j)] = -0.2288\,(17),$$
$$A_1[\mathrm{VI}(k)] = 0.6802\,(38).$$

VII. DISCUSSION

Let us first add up all terms contributing to $A_2^{(10)}(m_\mu/m_e)$ of muon g-2 evaluated by numerical integration. From (34), (34), (35), (39), (38), (41), (44), (47), and (49)–(57), which represent the contributions of 2958 Feynman diagrams belonging to 17 gauge-invariant sets, we obtain

$$A_2^{(10)}(m_\mu/m_e)[\text{partial sum}] = 662.50\,(27). \quad (61)$$

The uncertainties from these diagrams, which include all dominant sources of uncertainties considered previously, have been reduced to an insignificant level. Note, however, that some terms which were not included in previous estimates turned out to be not negligible.

Of course, the real value of $A_2^{(10)}(m_\mu/m_e)$ is not known until remaining diagrams are evaluated. However, they have no known mechanism for giving rise to large values and likely to remain modest in size and uncertainty. We therefore expect that the final value will stay within the range

$$A_2^{(10)}(m_\mu/m_e)[\text{estimate}] = 663\,(20). \quad (62)$$

This will reduce the previous value (16) by 1.81×10^{-11}. Our next step is to evaluate 6122 vertex diagrams from the remaining 14 gauge-invariant subsets. Many of these diagrams can be integrated by means of available information on Π and Λ. They include:

(1) Subsets I(f), I(g), I(h) of Set I.
(2) Subsets II(c), II(d) of Set II.
(3) Subsets III(a) and III(b) of Set III.
(4) All diagrams of Set IV, which can be evaluated by simple modification of codes of Group V of eighth-order diagrams.

These subsets are on our next time schedule. The remainder of diagrams are more difficult to evaluate for the following reasons:

(1) Subsets I(i) and I(j) require the knowledge of the eighth-order $v - p$ spectral function Π_8 which have not yet been constructed.
(2) Diagrams of Set II(e) require construction of radiatively-corrected light-by-light scattering subdiagrams, which are not yet available.
(3) Subset III[c] contains Λ_4 internally.
(4) Subsets VI(d), VI(g), and VI(h) have no lower-order structure upon which they can be built.

We foresee no intractable barrier for their evaluation.

As far as the electron $g - 2$ is concerned what is most important is the Set V which have no lower-order fermion loop structure. The integrands of this set are gigantic and require an enormous number of UV and IR subtraction terms. Our experience with the subsets VI(k) and VI(j) indicates, however, that their sizes are still manageable with available computers. What is really crucial for their evaluation, however, is that all steps of construction of integrand must be fully automated. Thus far we have succeeded in obtaining a code that handles renormalization of ultraviolet divergence automatically [50]. For the moment the infrared divergence is treated by giving a small cutoff mass λ to the photon. A code for cutoff-independent treatment of IR divergence is being developed.

ACKNOWLEDGMENTS

T. K.'s work is supported by the U.S. National Science Foundation under Grant No. PHY-0098631. T. K. thanks the Eminent Scientist Invitation Program of RIKEN, Japan, for the hospitality extended to him where a part of this work was carried out. T. K. is also supported during his stay

in Japan by Ministry of Education, Science and Culture of Japan, Grant-in-Aid for Scientific Research on Priority Areas, No. 13134101. M. N.'s work is partly supported by Japan Society for the Promotion of Science, Grant-in-Aid for Scientific Research (C) No. 15540303, 2003-2005. The numerical work has been carried out on the RIKEN Super Combined Cluster System (RSCC).

[1] P. Kusch and H. M. Foley, Phys. Rev. **72**, 1256 (1947).
[2] J. Schwinger, Phys. Rev. **73**, 416L (1948).
[3] W. E. Lamb, Sr. and R. C. Retherford, Phys. Rev. **72**, 241 (1947).
[4] A. Rich and J. C. Wesley, Rev. Mod. Phys. **44**, 250 (1972).
[5] R. S. Van Dyck, Jr., P. B. Schwinberg, and H. G. Dehmelt, Phys. Rev. Lett. **59**, 26 (1987).
[6] R. S. Van Dyck, Jr. *et al.* (unpublished).
[7] R. Mittleman, H. Dehmelt, and S. Kim, Phys. Rev. Lett. **75**, 2839 (1995).
[8] L. S. Brown, G. Gabrielse, K. Helmerson, and J. Tan, Phys. Rev. Lett. **55**, 44 (1985).
[9] B. Odom, Ph.D. thesis, Harvard University, 2005 (unpublished).
[10] A. Petermann, Helv. Phys. Acta **30**, 407 (1957).
[11] C. Sommerfield, Phys. Rev. **107**, 328 (1957).
[12] T. Kinoshita, Phys. Rev. Lett. **75**, 4728 (1995).
[13] S. Laporta and E. Remiddi, Phys. Lett. B **379**, 283 (1996).
[14] T. Kinoshita and M. Nio, Phys. Rev. D **73**, 013003 (2006).
[15] V. W. Hughes and T. Kinoshita, Rev. Mod. Phys. **71**, S133 (1999).
[16] F. Jegerlehner (private communication).
[17] B. Krause (private communication).
[18] A. Czarnecki, B. Krause, and W. J. Marciano, Phys. Rev. Lett. **76**, 3267 (1996).
[19] A. Wicht *et al.*, Phys. Scr. **T102**, 82 (2002).
[20] P. J. Mohr and B. N. Taylor, Rev. Mod. Phys. **77**, 1 (2005).
[21] J. Bailey *et al.*, Phys. Lett. B **68**, 191 (1977); F. J. M. Farley and E. Picasso, in *Quantum Electrodynamics*, edited by T. Kinoshita (World Scientific, Singapore, 1990), pp. 479–559.
[22] G. W. Bennett *et al.*, Phys. Rev. Lett. **92**, 161802 (2004).
[23] G. W. Bennett *et al.*, Phys. Rev. Lett. **89**, 101804 (2002).
[24] H. N. Brown *et al.*, Phys. Rev. Lett. **86**, 2227 (2001).
[25] H. N. Brown *et al.*, Phys. Rev. D **62**, 091101 (2000).
[26] A. Czarnecki and W. J. Marciano, Phys. Rev. D **64**, 013014 (2001).
[27] M. Davier and A. Höcker, Phys. Lett. B **435**, 427 (1998).
[28] S. Narison, Phys. Lett. B **513**, 53 (2001).
[29] J. F. de Troconiz and F. J. Yndurain, Phys. Rev. D **65**, 093001 (2002).
[30] M. Knecht and A. Nyffeler, Phys. Rev. D **65**, 073034 (2002); M. Knecht, A. Nyffeler, M. Perrottet, and E. de Rafael, Phys. Rev. Lett. **88**, 071802 (2002); M. Hayakawa and T. Kinoshita, hep-ph/0112102; J. Bijnens, E. Pallante, and J. Prades, Nucl. Phys. B **626**, 410 (2002); I. Blokland, A. Czarnecki, and K. Melnikov, Phys. Rev. Lett. **88**, 071803 (2002).
[31] M. J. Ramsey-Musolf and M. B. Wise, Phys. Rev. Lett. **89**, 041601 (2002).
[32] A. Höcker, hep-ph/0410081.
[33] K. Hagiwara, A. D. Martin, D. Nomura, and T. Teubner, Phys. Rev. D **69**, 093003 (2004).
[34] J. F. de Troconiz and F. J. Yndurain, Phys. Rev. D **71**, 073008 (2005).
[35] K. Melnikov and A. Vainshtein, Phys. Rev. D **70**, 113006 (2004).
[36] M. Knecht *et al.*, J. High Energy Phys. 11 (2002) 003.
[37] A. Czarnecki, W. J. Marciano, and A. Vainshtein, Phys. Rev. D **67**, 073006 (2003).
[38] T. Kinoshita and M. Nio, Phys. Rev. Lett. **90**, 021803 (2003).
[39] T. Kinoshita and M. Nio, Phys. Rev. D **70**, 113001 (2004).
[40] T. Kinoshita, Nucl. Phys. B (Proc. Suppl.) **144**, 206 (2005).
[41] S. Laporta, Phys. Lett. B **328**, 522 (1994).
[42] T. Kinoshita and W. J. Marciano, in *Quantum Electrodynamics*, edited by T. Kinoshita (World Scientific, Singapore, 1990), pp. 419–478.
[43] S. G. Karshenboim, Yad. Fiz. **56**, 252 (1993) [Phys. At. Nucl. **56**, 857 (1993)].
[44] A. S. Elikhovskii, Yad. Fiz. **49**, 1056 (1989) [Sov. J. Appl. Phys. **49**, 654 (1989)].
[45] A. L. Kataev, Phys. Lett. B **284**, 401 (1992).
[46] T. Kaneko, Comput. Phys. Commun. **92**, 127 (1995).
[47] S. Laporta and E. Remiddi, Phys. Lett. B **301**, 440 (1993).
[48] A. I. Milstein and A. S. Yelkhovsky, Phys. Lett. B **233**, 11 (1989).
[49] A. L. Kataev, hep-ph/0507174.
[50] T. Aoyama, M. Hayakawa, T. Kinoshita, and M. Nio, hep-ph/0512288.